bioRxiv preprint doi: https://doi.org/10.1101/2023.07.25.550448; this version posted July 25, 2023. The copyright holder for this preprint (which was not certified by peer review) is the author/funder, who has granted bioRxiv a license to display the preprint in perpetuity. It is made available under aCC-BY-NC-ND 4.0 International license.

VCF1 is an unconventional p97/VCP cofactor promoting recognition of ubiquitylated p97-UFD1-NPL4 substrates

Ann Schirin Mirsanaye[1,*], Saskia Hoffmann[1,*], Melanie Weisser[1], Andreas Mund[1], Blanca Lopez Mendez[1], Dimitris Typas[1], Johannes van den Boom[2], Bente Benedict[1], Ivo A. Hendriks[1], Michael Lund Nielsen[1], Hemmo Meyer[2], Julien P. Duxin[1], Guillermo Montoya[1], Niels Mailand[1,3,#]

[1]Protein Signaling Program, Novo Nordisk Foundation Center for Protein Research, University of Copenhagen, DK-2200 Copenhagen, Denmark; [2]Molecular Biology I, Faculty of Biology, University of Duisburg-Essen, 45117 Essen, Germany; [3]Center for Chromosome Stability, Department of Cellular and Molecular Medicine, University of Copenhagen, Blegdamsvej 3B, DK-2200 Copenhagen, Denmark

*Equal contribution; [#]Correspondence: niels.mailand@cpr.ku.dk

bioRxiv preprint doi: https://doi.org/10.1101/2023.07.25.550448; this version posted July 25, 2023. The copyright holder for this preprint (which was not certified by peer review) is the author/funder, who has granted bioRxiv a license to display the preprint in perpetuity. It is made available under aCC-BY-NC-ND 4.0 International license.

Summary

The hexameric AAA+ ATPase p97/VCP functions as an essential mediator of ubiquitin-dependent cellular processes, extracting ubiquitylated proteins from macromolecular complexes or membranes by catalyzing their unfolding. p97 is directed to ubiquitylated client proteins via multiple cofactors, most of which interact with the p97 N-domain. Here, we discovered that FAM104A, a protein of unknown function that we named VCF1 (VCP/p97 Cofactor FAM104 1), acts as a novel p97 cofactor in human cells. Detailed structure-function studies revealed that VCF1 directly binds p97 via a conserved novel α-helical motif that recognizes the p97 N-domain with unusually high affinity, exceeding that of other cofactors. We show that VCF1 engages in joint p97 complex formation with the heterodimeric primary p97 cofactor UFD1-NPL4 and promotes p97-UFD1-NPL4-dependent proteasomal degradation of ubiquitylated substrates in cells. Mechanistically, VCF1 indirectly stimulates UFD1-NPL4 interactions with ubiquitin conjugates via its binding to p97 but has no intrinsic affinity for ubiquitin. Collectively, our findings establish VCF1 as an unconventional p97 cofactor that promotes p97-dependent protein turnover by facilitating p97-UFD1-NPL4 recruitment to ubiquitylated targets.

bioRxiv preprint doi: https://doi.org/10.1101/2023.07.25.550448; this version posted July 25, 2023. The copyright holder for this preprint (which was not certified by peer review) is the author/funder, who has granted bioRxiv a license to display the preprint in perpetuity. It is made available under aCC-BY-NC-ND 4.0 International license.

Introduction

The highly abundant and evolutionarily conserved AAA+ ATPase Valosin-containing protein (VCP)/p97 (known as Cdc48 in lower eukaryotes) is a crucial mediator of ubiquitin-dependent processes and proteostasis mechanisms in eukaryotic cells, impacting and regulating most aspects of cell physiology [1,2]. The action of p97 principally entails the threading of, in most cases, ubiquitin-modified client proteins through the central pore of the barrel-shaped p97 homo-hexamer via two hexameric ATPase rings formed by the D1 and D2 ATPase domains within each p97 monomer. This leads to the unfolding of the substrate protein, enabling its degradation by the 26S proteasome or extraction from macromolecular complexes or cellular membranes [3-7]. The critical importance of p97 in cell and organismal physiology is underscored by the association of p97 mutations with neurodegenerative disorders including inclusion body myopathy with Paget's disease of bone and frontotemporal dementia (IBMPFD) and amyotrophic lateral sclerosis (ALS) [8]. On the other hand, targeting increased levels of proteotoxic stress in cancer cells using small molecule inhibitors of p97 represents a promising therapeutic avenue [9]. A detailed understanding of the workings of the p97 system is therefore of paramount biomedical importance.

Around 40 established cofactors are responsible for the interplay between p97 and its numerous cellular substrates, governing substrate recognition and specificity, subcellular localization and/or enzymatic activity of p97 complexes [2,10,11]. These cofactors directly interact with p97 via one or more well-defined domains and motifs, most of which recognize the p97 N-domain. Known p97 N-domain-binding modules include both globular UBX and UBX-like domains, which adopt a ubiquitin-like fold and interact with a large surface area on the N-domain, and short linear motifs including the SHP box and the VIM and VBM motifs [11]. While the SHP box binds the p97 N-domain close to the central pore and the D1 ATPase

bioRxiv preprint doi: https://doi.org/10.1101/2023.07.25.550448; this version posted July 25, 2023. The copyright holder for this preprint (which was not certified by peer review) is the author/funder, who has granted bioRxiv a license to display the preprint in perpetuity. It is made available under aCC-BY-NC-ND 4.0 International license.

domain, the VIM and VBM motifs adopt α-helical folds that enable them to dock into the hydrophobic cleft formed between the N- and C-terminal lobes of the p97 N-domain [11,12]. A considerable proportion of disease-associated p97 mutations map to the N-domain, highlighting the importance of p97-cofactor interactions for the proper functioning of the p97 system [8]. A smaller number of cofactors contain PUB or PUL domains that interact with the p97 C-terminus [11,12]. Many p97 cofactors also harbor one or more ubiquitin-binding domains that target p97 to ubiquitylated substrates, most of which are modified by K48-linked polyubiquitin chains [13]. In addition, some p97 cofactors contain enzymatic domains that impart further relevant functionalities such as ubiquitin chain editing activity to p97 complexes [12].

p97-cofactor interactions generally appear to be transient and highly dynamic [14], and while some major cofactors bind p97 in a mutually exclusive manner, different cofactors in many cases assemble jointly on individual p97 hexamers [12]. The regulatory mechanisms and hierarchies underlying the formation and dissociation of complexes between p97 hexamers and combinations of cofactors are not well understood, hampered by the complexity of the p97 system and the reliance on *in vitro* studies with purified proteins for characterizing this interplay. However, a general theme is that the basic functionality of p97-dependent processes is driven by primary p97 cofactors and augmented by accessory cofactors [15]. The heterodimeric UFD1-NPL4 complex defines one of the most important and best characterized primary p97 cofactors with a key role in unfolding ubiquitylated substrates. Recent elegant studies have provided detailed structural insight into how UFD1-NPL4 recruits p97 to ubiquitylated targets via multiple ubiquitin-binding domains, collaborating with p97 in a highly integrated fashion to unfold one of the ubiquitin molecules in the polyubiquitin chain attached to the substrate and initiate its unfolding via insertion into the p97 central pore [3,16,17].

bioRxiv preprint doi: https://doi.org/10.1101/2023.07.25.550448; this version posted July 25, 2023. The copyright holder for this preprint (which was not certified by peer review) is the author/funder, who has granted bioRxiv a license to display the preprint in perpetuity. It is made available under aCC-BY-NC-ND 4.0 International license.

This affords a general mechanism for the recognition and processing of p97 substrates that is independent of the ubiquitylated target protein itself. The efficiency of p97-UFD1-NPL4-dependent unfolding reactions can be further stimulated by accessory cofactors. For instance, recent work showed that ubiquitin-binding UBX-type cofactors including FAF1 and UBXN7 stabilize p97-UFD1-NPL4 interactions with K48-linked polyubiquitin chains, involving multivalent interactions between these proteins and ubiquitin chains that promote the coordinated assembly of p97-cofactor complexes on polyubiquitylated proteins [18,19]. These and other studies have made it clear that multi-layered cofactor-driven mechanisms underlie the productive processing of ubiquitylated p97 client proteins, and partial functional redundancies between individual cofactors appear to be a common feature of the p97 system, ensuring its efficacy in maintaining protein homeostasis and cell fitness under both basal and stressful conditions. Whether additional as-yet unidentified p97 cofactors with important roles in these processes exist remains to be seen.

In this study, we discovered a hitherto unrecognized vertebrate p97 cofactor that we named VCF1. We show that the interplay between VCF1 and p97 is mechanistically distinct from that of other cofactors, involving a novel α-helical motif that binds the p97 N-domain with unusually high affinity. VCF1 forms a joint complex with p97-UFD1-NPL4 and stimulates p97-UFD1-NPL4 interactions with ubiquitylated clients, promoting their turnover. However, VCF1 itself or in complex with p97 does not interact with ubiquitin, thus functioning as an unconventional accessory p97 cofactor that indirectly stimulates p97-UFD1-NPL4-dependent recognition and degradation of ubiquitylated target proteins via its tight binding to p97.

Results

bioRxiv preprint doi: https://doi.org/10.1101/2023.07.25.550448; this version posted July 25, 2023. The copyright holder for this preprint (which was not certified by peer review) is the author/funder, who has granted bioRxiv a license to display the preprint in perpetuity. It is made available under aCC-BY-NC-ND 4.0 International license.

VCF1 (FAM104A) is a p97-interacting protein

Through *in silico* searches for candidate regulators of p97 function, we came across FAM104A, a virtually uncharacterized protein detected in unbiased large-scale proteomic profiles of p97 interaction networks along with known p97 cofactors (**Figure S1A**) [20,21], but whose precise connection to p97 has not been studied. In humans, *FAM104A* encodes a relatively small protein of 186 amino acids that contains no annotated domains but is conserved across vertebrates (**Figure S1B**) and is broadly expressed, albeit at low levels, in human tissues. For reasons described in the following, we refer to FAM104A as VCF1 (VCP/p97 Cofactor FAM104 1). To investigate the function of VCF1, we generated cell lines expressing GFP-tagged VCF1 in a conditional manner, showing that VCF1 mainly localizes to the nucleoplasm (**Figure 1A,B**). We then performed mass spectrometry analysis of GFP pulldowns from these cells in order to profile the VCF1 interactome. Interestingly, this revealed a striking and highly selective enrichment of p97 (**Figure 1C; Figure S1C; Table S1, S2**). Notably, p97 efficiently co-precipitated with GFP-VCF1 under both mild and more stringent, partially denaturing RIPA buffer conditions (**Figure 1C; Figure S1C**), suggesting that VCF1 forms a tight complex with p97. We generated a VCF1 antibody and used this to validate an interaction between endogenous VCF1 and p97 (**Figure 1D**), supporting its physiological relevance. Moreover, purified recombinant VCF1 and p97 readily interacted *in vitro* (**Figure 1E; Figure S1D,E**), demonstrating that the association between these proteins is direct. Reciprocal co-IP analysis showed that the *Xenopus laevis* VCF1 ortholog interacted with p97 in *Xenopus* egg extracts (**Figure S1F**), indicating that the VCF1-p97 interaction is evolutionarily conserved. Using purified full-length and truncated p97 proteins, we asked which of its domains is required for binding to recombinant VCF1. This revealed that VCF1 interacts with the p97 N-domain, similar to the majority of known p97 cofactors (**Figure 1F,G; Figure S1G**) [11]. To further define the VCF1 binding site within the p97 N-domain, we

bioRxiv preprint doi: https://doi.org/10.1101/2023.07.25.550448; this version posted July 25, 2023. The copyright holder for this preprint (which was not certified by peer review) is the author/funder, who has granted bioRxiv a license to display the preprint in perpetuity. It is made available under aCC-BY-NC-ND 4.0 International license.

analyzed the impact of mutating a range of individual residues in this domain that have been shown by structural and biochemical studies to be important for interaction with different p97 cofactors [22]. We found that Y143 in p97, which is critical for binding several cofactors [22,23], was required for binding to VCF1 (**Figure 1E**), further confirming that VCF1 associates with the p97 N-domain. Having identified a p97 point mutation (Y143A) that abrogates VCF1 binding, we performed surface plasmon resonance (SPR) experiments to more quantitatively characterize the VCF1-p97 interaction. Strikingly, this showed that full-length VCF1 binds p97 with very high affinity (K_d ~10 nM) (**Figure 1H**), consistent with our VCF1 interactome studies above. In fact, the observed p97-binding affinity of VCF1 is substantially higher than those reported for other p97 cofactors, such as p47/NSFL1C (K_d in the ~200-500 nM range) [24,25]. As expected, the p97 Y143A mutant did not show detectable binding affinity for VCF1 in SPR experiments (**Figure 1H**). Together, these findings reveal VCF1 as a novel p97-binding protein that interacts tightly with the p97 N-domain.

VCF1 contains a novel high-affinity p97-binding motif

We next asked how VCF1 associates with p97. Most p97 cofactors contain one or more well-defined p97-interacting motifs, including the VIM, VBM and SHP short linear motifs and the UBX/UBX-like domains [11]. However, no sequences conforming to any of the known p97-interacting motifs were present in VCF1. To identify the p97-binding region in VCF1, we therefore used a series of overlapping peptides spanning the full-length VCF1 protein as baits in p97-binding experiments (**Figure 2A**). Incubation of these peptides with total cell extracts showed that the peptide encompassing the VCF1 C-terminus (VCF1-6) efficiently pulled down p97, whereas none of the other VCF1 peptides displayed detectable p97 binding (**Figure 2B**). Interestingly, this C-terminal portion of VCF1 harboring the p97-binding determinant represents its most highly conserved part and contains a region predicted by

bioRxiv preprint doi: https://doi.org/10.1101/2023.07.25.550448; this version posted July 25, 2023. The copyright holder for this preprint (which was not certified by peer review) is the author/funder, who has granted bioRxiv a license to display the preprint in perpetuity. It is made available under aCC-BY-NC-ND 4.0 International license.

AlphaFold2 [26] to adopt an α-helical fold, whereas the remaining VCF1 sequence is predicted to be mostly disordered (**Figure S1B; Figure S2A**). To more precisely delineate the p97-binding motif in the VCF1 C-terminus, we performed an alanine scan of residues within the predicted α-helix in the context of full-length VCF1. This revealed that N167, L170 and H174 are each essential for VCF1 binding to p97 (**Figure 2C**). Of note, these residues are all highly conserved among VCF1 orthologs and reside on the same face of the α-helix (**Figure 2D;** see also **Figure 3B**). Mass spectrometry-based comparison of the interactomes of stably expressed GFP-VCF1 wild-type (WT) and N167A mutant proteins further demonstrated that the N167A mutation led to a strong loss of p97 binding (**Figure 2E; Figure S2B,C; Table S3**). Moreover, *in vitro* binding experiments with purified proteins confirmed that the introduction of the N167A mutation in both full-length VCF1 and the VCF1-6 peptide abrogated binding to p97 (**Figure 2F; Figure S2D,E**). SPR experiments showed that the isolated VCF1 C-terminus binds p97 with a K_d of approx. 6 nM, comparable to our results for full-length VCF1 (**Figure 2F; Figure 1H**). These data show that VCF1 contains a novel type of linear motif mediating binding to p97 with unprecedented high affinity among p97 cofactors, which we refer to as the VRM (VCF1 p97-Recognizing Motif) (**Figure 2D**).

Structural modeling of the VCF1-p97 interaction

Having defined the primary sequence determinants in VCF1 and p97 underlying their association, we next sought to understand the structural basis of VCF1-p97 complex formation. Our attempts to obtain a cryo-EM structure of this complex were not successful, likely due to most of the VCF1 protein being disordered (**Figure S2A**), hence we used AlphaFold-Multimer [27] to model the VCF1-p97 interaction. This analysis revealed with high confidence that the VRM-containing α-helix in VCF1 docks at the interface between the two subdomains of the p97 N-domain involving N167, L170 and H174 in VCF1 and Y143 in p97

bioRxiv preprint doi: https://doi.org/10.1101/2023.07.25.550448; this version posted July 25, 2023. The copyright holder for this preprint (which was not certified by peer review) is the author/funder, who has granted bioRxiv a license to display the preprint in perpetuity. It is made available under aCC-BY-NC-ND 4.0 International license.

(**Figure 3A,B; Figure S3A**), in excellent agreement with our experimental data. This mode of binding bears significant resemblance to that reported for other p97-interacting motifs, in particular the VIM and VBM that also form α-helices [11,28]. Indeed, comparison of the AlphaFold-Multimer models for p97 N-domain binding to the VRM and other p97-interacting motifs suggested that VRM interacts with the cleft between the two lobes of the p97 N-domain in a manner that is similar but not identical to the VIM and VBM motifs (**Figure 3C**). The overlap between the N-domain surfaces recognized by the VRM and UBX domain is more limited, while the SHP box binds a distal region of the p97 N-domain that does not overlap with the VRM binding surface (**Figure S3B**) [11]. Consistent with both similarities and differences in the contacts made between p97 and the VRM, VIM and VBM motifs, Y143 in p97 was required for binding to all three motifs but not p47, whereas a number of other residues in the p97 N-domain known to make critical contacts with VIM and/or VBM [22] were dispensable for binding to VRM (**Figure 3D; Figure S3C**). Of note, the AlphaFold-Multimer models predicted that the surface area buried by VRM on the p97 N-domain is considerably larger than the corresponding one for the VIM and VBM motifs (~1100 Å^2 for VRM and ~750 Å^2 for VIM and VBM) (**Figure S3D**), in good agreement with the higher p97 binding affinity of VCF1 relative to other known p97 cofactors. Interestingly, crosslinking mass spectrometry analysis with purified proteins showed that a number of contacts are formed between VCF1 sequences N-terminal to the VRM and p97 (**Figure 3E; Figure S3E,F**), in accordance with the AlphaFold-Multimer model of the interaction between full-length VCF1 and p97 (**Figure S3A**). This suggests that in addition to high affinity p97 binding via the VRM a range of weaker contacts involving the intrinsically disordered region of VCF1 may also contribute to the VCF1-p97 interplay. Together with our findings above, these data illuminate the molecular basis of the VCF1-p97 interaction.

bioRxiv preprint doi: https://doi.org/10.1101/2023.07.25.550448; this version posted July 25, 2023. The copyright holder for this preprint (which was not certified by peer review) is the author/funder, who has granted bioRxiv a license to display the preprint in perpetuity. It is made available under aCC-BY-NC-ND 4.0 International license.

VCF1 and UFD1-NPL4 form a joint complex with p97

The notion that VCF1 and p97 cofactors containing VIM, VBM and UBX motifs recognize partially overlapping p97 N-domain surfaces suggests that they are mutually exclusive for binding to individual p97 monomers. However, VCF1 might form joint complexes with other cofactors on p97 hexamers. To address this possibility, we first used mass photometry to determine the stoichiometry of the VCF1-p97 interaction. This analysis suggested that, in the absence of other cofactors, 2-3 WT VCF1 molecules can bind a p97 hexamer (**Figure 4A**), which may permit other cofactors to associate with the VCF1-p97 complex. We performed *in vitro* binding experiments with purified proteins to examine this possibility for several p97 cofactors including UFD1-NPL4, p47 and FAF1. Moderate concentrations of VCF1 were clearly permissive for the simultaneous binding of VCF1 and UFD1-NPL4, p47 or FAF1 to p97, as evidenced by the presence of VCF1 in UFD1, p47 or FAF1 pulldowns that required its ability to bind p97 (**Figure 4B; Figure S4A-E**). Likewise, substantiating the formation of a joint p97-VCF1-UFD1-NPL4 complex, we found that UFD1-NPL4 co-purified with immobilized VCF1 in a manner that was fully dependent on the presence of p97 and the p97-binding proficiency of VCF1 (**Figure 4C; Figure S4F**). Gel filtration analysis provided further direct evidence for the formation of a stable complex between VCF1, UFD1-NPL4 and p97 (**Figure 4D**), and NPL4 could be detected in endogenous VCF1 IPs along with p97 (**Figure S4G; Figure S1F**). Since our mass photometry analysis suggested a stoichiometry of 2-3 bound VCF1 molecules per p97 hexamer (**Figure 4A**), we used AlphaFold-Multimer prediction to generate a model of a UFD1-NPL4-bound p97 hexamer that agrees with experimentally determined structures [29-31] and superimposed three VCF1 VRM-containing helices onto this model. No steric clashes were observed (**Figure S4H**), indicating that several copies of VCF1 should be able to associate with the p97-UFD1-NPL4 complex. We noticed that high concentrations of WT VCF1, but not the N167A mutant, displaced p47 and

bioRxiv preprint doi: https://doi.org/10.1101/2023.07.25.550448; this version posted July 25, 2023. The copyright holder for this preprint (which was not certified by peer review) is the author/funder, who has granted bioRxiv a license to display the preprint in perpetuity. It is made available under aCC-BY-NC-ND 4.0 International license.

UFD1-NPL4 from p97 *in vitro*, whereas increasing the concentration of p47 did not lead to dissociation of VCF1 from p97 (**Figure S4B,I,J**), consistent with the very high p97-binding affinity of VCF1. However, VCF1 is unlikely to displace UFD1-NPL4 or p47 from p97 under physiological conditions, as endogenous VCF1 is expressed at a low level in cells (~6,000 copies/HeLa cell) and is approximately 100-fold less abundant than both UFD1-NPL4 and p47, and 1,000-fold less abundant than p97 [32]. We conclude from these findings that VCF1 engages in complex formation with p97 together with other cofactors, including the primary p97 cofactor UFD1-NPL4.

VCF1 stimulates p97-UFD1-NPL4 recruitment to ubiquitylated clients to facilitate their degradation

UFD1-NPL4 is a major p97 cofactor complex with a crucial role in promoting p97-dependent unfolding of K48-ubiquitylated substrates to enable their proteasomal degradation [3,16,17]. To interrogate the functional relevance of the observed complex formation between VCF1 and p97-UFD1-NPL4, we asked whether and how VCF1 status impacts the degradation of the well-established p97-UFD1-NPL4 model substrate Ub(G76V)-GFP that reflects the properties of an endogenous p97 target [33] in cells stably expressing this fusion protein. The level of Ub(G76V)-GFP is normally kept extremely low due to its constitutive poly-ubiquitylation and ensuing p97-UFD1-NPL4- and proteasome-dependent degradation but can be efficiently stabilized by inhibition of p97 or the proteasome (**Figure S5A**) [34,35]. Depletion of NPL4 increased Ub(G76V)-GFP abundance as expected, whereas knockdown of p47, which has not been implicated in Ub(G76V)-GFP degradation, had no effect (**Figure 5A,B; Figure S5B**). Of note, we could only achieve partial knockdown of NPL4 (**Figure S5B**), likely due to its essential role in p97-dependent protein degradation [15]. Interestingly, knockdown of VCF1 by two independent siRNAs stabilized Ub(G76V)-GFP to a similar

bioRxiv preprint doi: https://doi.org/10.1101/2023.07.25.550448; this version posted July 25, 2023. The copyright holder for this preprint (which was not certified by peer review) is the author/funder, who has granted bioRxiv a license to display the preprint in perpetuity. It is made available under aCC-BY-NC-ND 4.0 International license.

extent as reducing NPL4 levels (**Figure 5A,B; Figure S5B**), suggesting that VCF1 is functionally involved in the p97-UFD1-NPL4-dependent processing of ubiquitylated proteins. By contrast, VCF1 depletion had a marginal impact on levels of a variant Ub(G76V)-GFP-20AA substrate that does not require p97 activity for its proteasomal degradation [34,36] (**Figure S5A,C**), consistent with VCF1 acting at the p97-dependent step of Ub(G76V)-GFP turnover. Remarkably, co-depletion of VCF1 and NPL4, but not p47, led to a dramatic accumulation of Ub(G76V)-GFP that greatly exceeded the impact of individual VCF1 or NPL4 knockdown (**Figure 5A,B; Figure S5B**). Moreover, when Ub(G76V)-GFP was allowed to accumulate to high levels by treatment with a p97 inhibitor (p97i), depletion of VCF1 delayed the p97-dependent clearance of Ub(G76V)-GFP following p97i removal (**Figure S5D**). Thus, under conditions of reduced NPL4 availability or a high demand for p97 activity, VCF1 becomes crucial for p97-UFD1-NPL4-dependent turnover of ubiquitylated substrates. During unperturbed growth, however, VCF1 depletion only had a modest impact on steady-state levels of ubiquitin conjugates and cell proliferation (**Figure S5E,F**). Overexpression of WT VCF1, but not the p97 binding-deficient N167A mutant, also stabilized Ub(G76V)-GFP similar to the effect of elevating NPL4 or p47 expression levels (**Figure S5G**), suggesting that a carefully controlled balance of p97 interactions with VCF1 and other cofactors is critical for the efficient processing of ubiquitylated substrates.

We next addressed how VCF1 stimulates p97-UFD1-NPL4-dependent protein degradation. The binding of VCF1 had no impact on the ATPase activity of p97 *in vitro* (**Figure S5H**). Prompted by recent work showing that UBX-type accessory p97 cofactors including FAF1 and UBXN7 stabilize p97-UFD1-NPL4 interactions with K48-linked ubiquitin chains [18,19], we considered the possibility that VCF1 may similarly enhance p97-UFD1-NPL4 binding to ubiquitylated client proteins. Indeed, using purified proteins we found that WT VCF1 had a

bioRxiv preprint doi: https://doi.org/10.1101/2023.07.25.550448; this version posted July 25, 2023. The copyright holder for this preprint (which was not certified by peer review) is the author/funder, who has granted bioRxiv a license to display the preprint in perpetuity. It is made available under aCC-BY-NC-ND 4.0 International license.

strong stimulatory impact on p97-UFD1-NPL4 binding to K48-linked poly-ubiquitin chains *in vitro* (**Figure 5C; Figure S5I**). Substantiating this notion, we observed a similar prominent ability of VCF1 to enhance p97-UFD1-NPL4 binding to ubiquitylated proteins in total cell extracts (**Figure 5D**). Importantly, this effect was abrogated by mutation of the VRM (**Figure 5C,D**), demonstrating that the VCF1-dependent stabilization of complexes between p97-UFD1-NPL4 and ubiquitin chains requires its binding to p97. Strikingly, however, neither in isolation nor in complex with p97 did VCF1 display detectable interaction with ubiquitin unlike most p97 cofactors (**Figure 5D,E; Figure S5J**). Moreover, VCF1 harbors no sequences conforming to known ubiquitin-binding domains, further arguing against a direct role of VCF1 in recruiting p97 to ubiquitylated substrates. Using truncated VCF1 proteins, we found that the C-terminal portion harboring the VRM was sufficient to enhance p97-UFD1-NPL4 interactions with ubiquitin conjugates (**Figure S5K**), suggesting that the binding of VCF1 to p97 *per se* represents a primary determinant for its stimulatory impact on p97-UFD1-NPL4 binding to ubiquitylated substrates. Consistent with this scenario, VCF1 did not directly interact with UFD1-NPL4 and had no discernible impact on UFD1-NPL4 association with p97 (**Figure 4B,C; Figure 5C**). Importantly, using ubiquitin binding-deficient UFD1 and NPL4 mutants [18,37,38] we established that the ability of VCF1 to boost p97-UFD1-NPL4 interactions with ubiquitylated proteins is fully dependent on the ubiquitin-binding ability of the UFD1-NPL4 complex (**Figure 5E**), further demonstrating that the VCF1-p97 complex has no overt ubiquitin-binding ability on its own. Together, these data suggest that VCF1 promotes p97-dependent protein degradation by stimulating the interaction of p97-UFD1-NPL4 with ubiquitylated substrates, via an unconventional mechanism differing from that of UBX-type cofactors by being principally mediated by the direct binding of VCF1 to p97 but not ubiquitin (**Figure 5F**).

bioRxiv preprint doi: https://doi.org/10.1101/2023.07.25.550448; this version posted July 25, 2023. The copyright holder for this preprint (which was not certified by peer review) is the author/funder, who has granted bioRxiv a license to display the preprint in perpetuity. It is made available under aCC-BY-NC-ND 4.0 International license.

Discussion

p97 is a nexus of the ubiquitin system, unfolding numerous ubiquitylated client proteins recruited by a broad range of cofactors. Here, we discovered that the small uncharacterized protein VCF1 defines a hitherto unrecognized p97 cofactor, displaying several unique features that set it apart from known cofactors. Our detailed biochemical and biophysical analyses revealed that VCF1 directly binds p97 with unusually high affinity relative to other cofactors, and that this is mediated by a novel α-helical motif (VRM) that forms extensive contacts with the p97 N-domain. As VCF1 is a low-abundant protein whose copy number in HeLa cells is approx. 1,000-fold lower than p97 [32], it is likely that a large fraction of the endogenous VCF1 pool is constitutively associated with p97. Indeed, despite its low abundance the binding of VCF1 to p97 could be readily observed at the endogenous level, supporting the physiological importance of this interaction. Although VCF1 binds p97 with very high affinity by recognizing a surface on the p97 N-domain that partially overlaps with that of other p97-binding motifs, the VCF1-p97 complex is permissive for the simultaneous binding of additional N-domain-binding cofactors, as only 2-3 VCF1 molecules associate with a p97 hexamer even under saturating concentrations. We established that VCF1 forms a joint complex with UFD1-NPL4 on p97, and that this is functionally important for promoting p97-UFD1-NPL4-dependent turnover of a ubiquitylated model substrate in cells. Mechanistically, we show that VCF1 acts in an unorthodox way to stimulate p97-UFD1-NPL4 binding to poly-ubiquitylated proteins via the ubiquitin-binding motifs of UFD1 and NPL4. In terms of the functional outcome, this mechanism of action shares features with that recently described for ubiquitin-binding UBX-type p97 cofactors including FAF1 and UBXN7, which stabilize p97-UFD1-NPL4 interactions with K48-linked polyubiquitin chains to promote ubiquitin-dependent unloading of the replicative CMG helicase from chromatin

bioRxiv preprint doi: https://doi.org/10.1101/2023.07.25.550448; this version posted July 25, 2023. The copyright holder for this preprint (which was not certified by peer review) is the author/funder, who has granted bioRxiv a license to display the preprint in perpetuity. It is made available under aCC-BY-NC-ND 4.0 International license.

[18,19]. Thus, like these UBX-type cofactors, VCF1 promotes the targeting of p97 to ubiquitylated client proteins in a substrate-agnostic manner by enhancing the affinity of p97-UFD1-NPL4 for poly-ubiquitin modifications (**Figure 5F**). However, contrary to the UBX proteins, VCF1 does not possess detectable intrinsic ubiquitin-binding ability but instead augments the ubiquitin-binding affinity of the p97-bound UFD1-NPL4 complex indirectly. We found that this is primarily mediated by the docking of the VRM on the p97 N-domain, which is necessary and sufficient for enhancing the ubiquitin-binding capacity of the p97-UFD1-NPL4 complex. In line with the VRM providing a principal contribution to stimulating p97-UFD1-NPL4 interactions with ubiquitin chains, most of the VCF1 sequence apart from the VRM-containing α-helix is relatively poorly conserved among vertebrates (**Figure S1B**). However, using crosslinking mass spectrometry we found that the intrinsically disordered portion of VCF1 also makes a number of contacts to p97. This suggests that in addition to the tight VRM-p97 N-domain association multivalent low-affinity VCF1-p97 interactions involving sequences outside the VRM may also be relevant for the role of VCF1 in regulating p97 functions in cells, analogous to previous findings for disordered regions within the p97 cofactor UBXD1 [39]. Elucidating the precise molecular basis of how VCF1 binding to the p97 N-domain impacts the configuration of the p97-UFD1-NPL4 complex to enhance its interaction with ubiquitin chains will ultimately require structural insights, which may be challenging given the intrinsically disordered nature of most of the VCF1 protein.

The complementary mechanisms of action of VCF1 and UBX-type cofactors in enhancing p97-UFD1-NPL4 interactions with ubiquitylated target proteins may be an important component of multi-layered processes ensuring the robustness and flexibility of the p97 system in unfolding large swathes of ubiquitylated client proteins throughout the cell. We found that when the availability of p97-UFD1-NPL4 is restricted by partial depletion of

bioRxiv preprint doi: https://doi.org/10.1101/2023.07.25.550448; this version posted July 25, 2023. The copyright holder for this preprint (which was not certified by peer review) is the author/funder, who has granted bioRxiv a license to display the preprint in perpetuity. It is made available under aCC-BY-NC-ND 4.0 International license.

NPL4, VCF1 becomes instrumental for turning over the p97-UFD1-NPL4 model substrate Ub(G76V)-GFP. Moreover, high levels of Ub(G76V)-GFP requires VCF1 function for efficient p97-dependent clearance. During unperturbed conditions, however, depletion of VCF1 has little impact on overall levels of ubiquitin conjugates and cell fitness. This suggests that VCF1 and other cofactors may have at least partially redundant roles in stimulating p97-UFD1-NPL4 interactions with and processing of ubiquitylated targets under steady-state conditions where the basal activity of this complex is not rate-limiting, whereas individual cofactors may become more critical when demand for p97-UFD1-NPL4-mediated protein unfolding and degradation surges. Whether VCF1 acts as a general mediator of p97-UFD1-NPL4-dependent protein turnover, as might be suggested by the apparent lack of domains other than its conserved p97-binding motif, or promotes p97-UFD1-NPL4 function in specific contexts remains to be established. However, given its high affinity for p97 binding it seems likely that VCF1 is a preferred accessory cofactor for enhancing the basal ubiquitin-binding capacity of the p97-UFD1-NPL4 complex. Indeed, VCF1 depletion had a much stronger impact on Ub(G76V)-GFP levels than FAF1 knockdown. Given that only one UFD1-NPL4 heterodimer associates with each p97 hexamer [12], it is also possible that VCF1 may shield free p97 N-domains in the p97-UFD1-NPL4 complex from binding by cofactors antagonizing the action of p97-UFD1-NPL4 in unfolding ubiquitylated substrates. Irrespective of the precise mechanism, our studies show that the ratio between VCF1 and other p97 cofactors must be carefully balanced to ensure proper functionality of p97-UFD1-NPL4-dependent protein degradation. The tight p97 binding of VCF1 could make it pertinent for its expression levels to be kept low to avoid disrupting such equilibria. At present, the mechanisms controlling p97-cofactor interactions are not well understood but are likely subject to a considerable degree of regulatory complexity given the multitude of p97

bioRxiv preprint doi: https://doi.org/10.1101/2023.07.25.550448; this version posted July 25, 2023. The copyright holder for this preprint (which was not certified by peer review) is the author/funder, who has granted bioRxiv a license to display the preprint in perpetuity. It is made available under aCC-BY-NC-ND 4.0 International license.

functions and cofactors. Future studies of the biological role of VCF1 may shed important further light on the workings and regulation of the p97 system.

Methods

Cell culture

U2OS and HEK293-6E cells were obtained from ATCC. All mammalian cell lines were cultured under standard conditions at 37 °C and 5% CO_2 in DMEM (Thermo) supplemented with 10% FBS (v/v) and penicillin-streptomycin (Thermo). Recombination cloning-compatible U2OS cells were generated using the Flp-In T-Rex Core Kit (Thermo) according to the manufacturer's instructions and maintained under selection using Blasticidin (Invivogen) and Zeocin (Thermo). To generate cell lines stably expressing GFP-VCF1, U2OS(FlpIn) cells were co-transfected with GFP-VCF1 constructs and pOG44 (Thermo) plasmids, followed by selection with Hygromycin (Invitrogen). Single clones were carefully screened for uniform expression of ectopic GFP-VCF1 at low levels and maintained under selection with blasticidin and hygromycin. To induce GFP-VCF1 expression, cells were treated with Doxycycline (DOX) (0.5 µg/ml) for 16 h. U2OS cell lines stably expressing Ub(G76V)-GFP or Ub(G76V)-GFP-20AA were described previously [40]. All cell lines used in this study were regularly tested negative for mycoplasma infection and were not authenticated.

Relative cell proliferation was measured using an Incucyte S3 Live-Cell Analysis System. Cells were treated with indicated siRNAs 36 h prior to seeding. Cells (2×10^4) were seeded in triplicate into a 12-well plate. Cells were imaged at 6-h intervals with a mean confluency determined from 9 images per well.

bioRxiv preprint doi: https://doi.org/10.1101/2023.07.25.550448; this version posted July 25, 2023. The copyright holder for this preprint (which was not certified by peer review) is the author/funder, who has granted bioRxiv a license to display the preprint in perpetuity. It is made available under aCC-BY-NC-ND 4.0 International license.

Unless otherwise indicated, the following drug concentrations were used: NMS-873 (p97i; 5 μM, Sigma), MG132 (20 μM; Sigma).

Xenopus egg extracts

Nucleoplasmic egg extracts (NPE) were prepared using *Xenopus laevis* (LM0053MX, LM00715MX, Nasco). All experiments involving animals were approved by the Danish Animal Experiments Inspectorate and conform to relevant regulatory standards and European guidelines. Preparation of *Xenopus* egg extracts was performed as described previously [41,42].

Plasmids and siRNAs

Bacterial expression constructs for His_6-tagged p97 fragments were generated by Q5 Site-Directed mutagenesis (New England Biolabs) of pET15b-His_6-p97 plasmid, using the following primers: 5′-TGACGATATCATGGCTTCTGGAGCC-3' and 5'-TGACGCGGCCGCCTAGCCATACAGGTCA-3' (for full-length p97); 5'-TGACGCGGCCGCCTATTCGCAGTGGATCACTGTG-3' (for p97 N); 5'-TGACGCGGCCGCCTAGCCCCCGATGTCTTC-3' (for p97 N+D1); 5'-TGACGATATCAAGCAGCTAGCTCAG-3' (for p97 D1+D2). Mammalian expression constructs for GFP-VCF1 WT and Strep-HA-VCF1 were generated by PCR amplification of a synthetic *VCF1* cDNA isoform (Thermo Fisher Scientific) encoding isoform 1 of human FAM104A (UniProt ID: Q969W3) and insertion into pcDNA5/FRT/TO/EGFP or pcDNA5/FRT/TO/Strep-HA (Thermo), respectively, using KpnI and ApaI. Mammalian expression construct for FLAG-VCF1 was generated by inserting *VCF1* cDNA into p-FLAG-CMV-2 (Sigma). Point mutations were introduced using the Q5 Site-Directed Mutagenesis kit (New England Biolabs). pET41b+_Ufd1-His_6 (#117107), pET41b+_Npl4 (#117108) and pcDNA5/FRT/TO-FAF1-Strep-HA (#113486) were acquired from Addgene. Ubiquitin binding-deficient (*UBD) mutants of UFD1-His_6 (deletion of amino acids 2-215) and NPL4

bioRxiv preprint doi: https://doi.org/10.1101/2023.07.25.550448; this version posted July 25, 2023. The copyright holder for this preprint (which was not certified by peer review) is the author/funder, who has granted bioRxiv a license to display the preprint in perpetuity. It is made available under aCC-BY-NC-ND 4.0 International license.

(T590L+F591V point mutations) [18] were generated using the Q5 Site-Directed Mutagenesis kit (New England Biolabs).

All siRNAs (Sigma) were used at 20 nM and transfected with Lipofectamine RNAiMAX reagent (Thermo) according to manufacturer's instructions. The following siRNA oligonucleotides were used: Non-targeting control (CTRL): 5′-GGGAUACCUAGACGUUCUA-3′; VCF1(#1): 5'-GACAGUGGUGGGAGCAGCA-3'; VCF1(#2): 5'-GUCUUCAGGCAGUGACAGU-3'; p47: 5'-AGCCAGCUCUUCCAUCUUA-3'; NPL4: 5'-CACGCCUAAUCCUGUUGACAA-3'; FAF1: 5′-CCACCUUCAUCAUCUAGUC-3′; p97: Dharmacon SmartPool (D-008727).

Expression and purification of recombinant proteins

His_6-p97, His_6-p47 and FLAG-p97 proteins were expressed in chemically competent *E. coli* BL21(DE3) (Thermo Fisher Scientific) by adding 1 mM IPTG (AppliChem) for 3 h at 37 °C. Bacterial pellets were then lysed in low salt buffer (50 mM Tris-HCl, pH 7.5; 0.2 M NaCl; 10% Glycerol; 10 mM Imidazole; 0.1% Triton-X100; 2 mM DTT) containing protease inhibitors, and lysates were sonicated and cleared by centrifugation. Cleared lysates were incubated with equilibrated Ni-NTA beads (Qiagen), incubated for 2 h at 4 °C, washed in a gravity column using 100 ml high salt buffer (50 mM Tris-HCl, pH 7.5; 1 M NaCl; 10% Glycerol; 15 mM Imidazole; 0.1% Triton-X100; 2 mM DTT) and 75 ml low salt buffer, followed by elution using low salt buffer containing 350 mM imidazole (His_6-p97 and His_6-p47), or incubated with equilibrated FLAG beads (anti-FLAG M2 Affinity Gel, Sigma Aldrich), incubated for 2 h at 4 °C washed in a gravity column using 150 ml lysis buffer, followed by elution using lysis buffer containing 0.5 mg/ml 3X FLAG Peptide (Sigma Aldrich) (FLAG-p97). The elute fractions were run on a 4-12% NuPAGE Bis-Tris protein gel (Invitrogen) and stained with Instant Blue Coomassie Protein Stain (Expedeon). Fractions were concentrated on Microcon-30 kDa Centrifugal Filters (Millipore), pooled and loaded

bioRxiv preprint doi: https://doi.org/10.1101/2023.07.25.550448; this version posted July 25, 2023. The copyright holder for this preprint (which was not certified by peer review) is the author/funder, who has granted bioRxiv a license to display the preprint in perpetuity. It is made available under aCC-BY-NC-ND 4.0 International license.

onto a Superose 6 10/300 GL column equilibrated in gel filtration buffer (20 mM HEPES, pH 7.5; 150 mM NaCl; 2 mM DTT). Fractions containing His_6-p97, His_6-p47 or FLAG-p97 were then pooled, concentrated, aliquoted and snap-frozen in liquid nitrogen.

For expression and purification of Strep-HA-VCF1 proteins, HEK293-6E suspension cells were cultured in FreeStyle F17 expression medium (Gibco) supplemented with 4 mM L-glutamine (Gibco), 1% FBS, 0,1% Pluronic F-68 (Gibco) and 50 µg/ml G418 (Invivogen) in a 37 °C incubator on a shaker rotating at 140 rpm. Cells were transfected with Strep-HA-VCF1 expression plasmids using PEI transfection reagent (Polyscience Inc). After 30 h, cells were harvested and snap-frozen in liquid nitrogen. The cell pellet was resuspended in lysis buffer (100 mM Tris, pH 8.0; 350 mM NaCl; 0,05% NP-40 and protease inhibitors), treated with benzonase and sonicated. The lysate was cleared by centrifugation at 25,000 g at 4 °C for 30 min and incubated with Strep-Tactin Superflow resin (IBA) at 4 °C for 2 h. Beads were washed in a gravity column using wash buffer (100 mM Tris pH 8.0; 600 mM NaCl; 0,05% NP-40) and Strep-HA-VCF1 protein was eluted using elution buffer (100 mM Tris pH 8.0; 350 mM NaCl; 2,5 mM Desthiobiotin (IBA)). The elute fractions were run on a 4-12% NuPAGE Bis-Tris protein gel (Invitrogen) and stained with Instant Blue Coomassie Protein Stain (Expedeon). Fractions were concentrated on Microcon-10 kDa Centrifugal Filters (Millipore), pooled and loaded onto a Superose 6 10/300 GL column equilibrated in gel filtration buffer (20 mM HEPES, pH 7.5; 150 mM NaCl; 2 mM DTT). Fractions containing VCF1 were then pooled, concentrated, aliquoted and snap-frozen in liquid nitrogen.

UFD1-His_6-NPL4 complex was expressed and purified as described previously [19]. Briefly, NPL4 and UFD1-His_6 proteins were expressed individually (ratio 2:1) overnight at 18 °C in chemically competent *E. coli* BL21(DE3) (Thermo Fisher Scientific) by addition of 1 mM IPTG (AppliChem). Bacterial pellets were resuspended in lysis buffer (50 mM Tris-HCl, pH

bioRxiv preprint doi: https://doi.org/10.1101/2023.07.25.550448; this version posted July 25, 2023. The copyright holder for this preprint (which was not certified by peer review) is the author/funder, who has granted bioRxiv a license to display the preprint in perpetuity. It is made available under aCC-BY-NC-ND 4.0 International license.

8.0; 0.5 M NaCl; 5 mM $Mg(OAc)_2$; 0.5 mM TCEP; 30 mM imidazole) containing protease inhibitors. The samples were then mixed, supplemented with lysozyme (Fisher Scientific) and sonicated before clearing the lysates by centrifugation. The supernatant was mixed with Ni-NTA beads (Qiagen), incubated for 2 h at 4 °C and the beads washed in a gravity column using 150 ml lysis buffer, followed by 10 ml of lysis buffer containing 50 mM imidazole, 2 mM ATP and 10 mM $Mg(OAc)_2$. The protein complex was then eluted in lysis buffer containing 400 mM imidazole. The elute fractions were run on a 4-12% NuPAGE Bis-Tris protein gel (Invitrogen) and stained with Instant Blue Coomassie Protein Stain (Expedeon). Fractions were concentrated on Microcon-10 kDa Centrifugal Filters (Millipore), pooled and loaded onto a Superose 6 10/300 GL column equilibrated in UFD1-NPL4 gel filtration buffer (20 mM HEPES-KOH, pH 7.9; 150 mM NaCl; 5 mM $Mg(OAc)_2$; 0.3 M sorbitol; 0.5 mM TCEP). Fractions containing the UFD1-His_6-NPL4 complex were then pooled, concentrated, aliquoted and snap-frozen in liquid nitrogen.

For purification of NPL4-GST-UFD1 complex, NPL4 and GST-UFD1 were expressed individually (ratio 2:1) in chemically competent *E. coli* BL21(DE3) (Thermo Fisher Scientific) by addition of 1 mM IPTG (AppliChem) for 3 h at 37 °C. Bacterial pellets were then mixed and lysed in lysis buffer (50 mM HEPES-KOH, pH 7.5; 150 mM KCl; 5% Glycerol; 2 mM $MgCl_2$; 0.5 mM TCEP) containing protease inhibitors, treated with lysozyme (Fisher Scientific), and lysates were sonicated and cleared by centrifugation. The cleared lysates were incubated with equilibrated Glutathione agarose (Gold Biotechnology) for 2 h at 4 °C and the beads washed in a gravity column using 50 ml lysis buffer, 50 ml high salt buffer (lysis buffer containing 300 mM KCl) and 50 ml lysis buffer. Proteins were eluted by adding lysis buffer containing 35 mM reduced glutathione (Gold Biotechnology). The elute fractions were run on a 4-12% NuPAGE Bis-Tris protein gel (Invitrogen) and stained with Instant Blue Coomassie Protein Stain (Expedeon). Fractions were concentrated on Microcon-

bioRxiv preprint doi: https://doi.org/10.1101/2023.07.25.550448; this version posted July 25, 2023. The copyright holder for this preprint (which was not certified by peer review) is the author/funder, who has granted bioRxiv a license to display the preprint in perpetuity. It is made available under aCC-BY-NC-ND 4.0 International license.

30 kDa Centrifugal Filters (Millipore), pooled and loaded onto a Superose 6 10/300 GL column equilibrated in NPL4-GST-UFD1 gel filtration buffer (50 mM HEPES pH 7.5; 150 mM KCl; 2 mM $MgCl_2$; 0.5 mM TCEP). Fractions containing the NPL4-GST-UFD1 complex were then pooled, concentrated, aliquoted and snap-frozen in liquid nitrogen.

Antibodies

The following commercial antibodies were used: FLAG (A00187, GenScript, mouse, 1:1000); HA (11867423001, Roche, rat, 1:1000); HA (sc-7392, Santa Cruz, mouse, 1:1000); HA (sc-805, Santa Cruz, rabbit, 1:1000); HA (MMS-101R, Covance, mouse, 1:1000); His_6 (631212, Clontech, mouse, 1:500); NPL4 (sc-365796, Santa Cruz, mouse, 1:500); NPL4 (HPA021560, Atlas Antibodies, rabbit, 1:1000); (UFD1 (sc-136114, Santa Cruz, mouse, 1:500); UFD1 (611642, BD Biosciences, mouse, 1:1000); Ubiquitin (43124S, Cell Signaling Technology, rabbit, 1:1000); Ubiquitin (sc-8017, Santa Cruz, mouse, 1:1000); p97 (MA3-004, Invitrogen, mouse, 1:5.000); p97: Santa Cruz, mouse, sc-57492); GST (sc-138, Santa Cruz, mouse, 1:1000); p47 (NBP213677, Novus Biologicals, rabbit, 1:1000). A sheep polyclonal VCF1 antibody was raised against full-length human VCF1 by MRC PPU Reagents and Services (University of Dundee, UK) and used at a 1:200 dilution. Antibodies against *Xenopus* p97, NPL4 and UFD1 [43] were a kind gift from Olaf Stemmann (University of Bayreuth, Germany). The following antibodies against *Xenopus* proteins were raised against the indicated peptides (New England Peptide): VCF1 N-terminus (H2N-MLPDSRKRRRNSNEVSEC-amide), VCF1 C-terminus (Aoa-KEAHFSSLQQRCCNSS-OH). The VCF1 antibody used for immunoblotting was raised against full-length *Xenopus laevis* VCF1 (Biogenes). The VCF1 protein was tagged with His_6 on the N-terminus and purified under denaturing conditions.

Cell lysis, immunoblotting and immunoprecipitation

bioRxiv preprint doi: https://doi.org/10.1101/2023.07.25.550448; this version posted July 25, 2023. The copyright holder for this preprint (which was not certified by peer review) is the author/funder, who has granted bioRxiv a license to display the preprint in perpetuity. It is made available under aCC-BY-NC-ND 4.0 International license.

Immunoblotting was performed as previously described [44]. Immunoprecipitation (IP) of HA-tagged proteins was performed using Anti-HA Affinity matrix (Roche) under denaturing conditions, unless otherwise stated. GFP-trap and DYKDDDDK Fab-trap agarose (Chromotek) were used according to manufacturer's instructions. Cell lysis was performed using RIPA buffer (140 mM NaCl; 10 mM Tris-HCl, pH 8.0; 0.1% sodium deoxycholate; 1% Triton X-100; 0.1% SDS; 1 mM EDTA; 0.5 mM EGTA) or EBC buffer (50 mM Tris, pH 7.5; 150 mM NaCl; 1 mM EDTA; 0.5% NP-40, 1 mM DTT). IPs were washed in non-denaturing buffer (50 mM Tris-HCl, pH 7.5; 150 mM NaCl; 0.5 mM EDTA). Cell lysis and IP under partially denaturing conditions were performed using denaturing buffer (20 mM Tris-HCl, pH 7.5; 50 mM NaCl; 0.5% sodium deoxycholate; 0.5% NP-40; 0.5% SDS; 1 mM EDTA). All lysis and wash buffers were supplemented with 1 mM fresh PMSF Protease Inhibitor (Thermo), complete EDTA-free protease inhibitor Cocktail Tablets (Roche), 1.25 mM N-ethylmaleimide (Sigma) and 50 µM PR-619 (Calbiochem).

To immunodeplete VCF1, p97 and NPL4 from *Xenopus* egg extracts, one volume of Protein A Sepharose beads (GE Healthcare) was mixed with two volumes of VCF1 N-terminus (1 mg/ml), VCF1 C-terminus (1 mg/ml), p97 and NPL4 antibodies and incubated overnight at 4 °C. After incubation, beads were washed 4 times with ELB buffer (10 mM HEPES, pH 7.7; 50 mM KCl; 2.5 mM $MgCl_2$; 250 mM sucrose). One volume of NPE was mixed with one volume of beads for 1 h at room temperature. Supernatant samples were harvested and beads were washed 4 times using ELB buffer containing 0,25% NP-40 and resuspended in 2x Laemmli sample buffer.

Immunofluorescence

Mammalian cells grown on coverslips were fixed in formalin buffer (VWR) for 15 min at room temperature (RT). Cells were permeabilized with PBS containing 0.5% Triton-X for 5 min and blocked with 5% BSA (Sigma) for 1 h prior to staining with indicated primary

bioRxiv preprint doi: https://doi.org/10.1101/2023.07.25.550448; this version posted July 25, 2023. The copyright holder for this preprint (which was not certified by peer review) is the author/funder, who has granted bioRxiv a license to display the preprint in perpetuity. It is made available under aCC-BY-NC-ND 4.0 International license.

antibodies for 1 h at RT. After 3 washes cells were stained with a combination of Alexa Fluor secondary antibodies and 4′,6-Diamidino-2-Phenylindole (DAPI; Molecular Probes) for 1 h at room temperature in the dark. Finally, after 4 further rounds of washing, coverslips were dried and mounted on glass slides using Mowiol (Sigma). Quantitative image-based cytometry (QIBC) was performed as described [45]. In brief, cells were fixed, permeabilized and stained as described above. Images were acquired with a ScanR high-content screening microscope (Olympus). Automated and unbiased image analysis was carried out with the ScanR analysis software (version 2.8.1). Data were exported and processed using Spotfire software (version 10.5.0; Tibco).

In vitro binding experiments

All *in vitro* binding experiments were performed in EBC or RIPA buffer as indicated. Recombinant Biotin-tagged K48-linked poly-ubiquitin chains (2-7) and K48-linked poly-ubiquitin chains (2-16) were purchased from R&D Systems and Enzo Life Science, respectively. Recombinant proteins were incubated with Strep-Tactin Sepharose (IBA), Glutathione agarose (Gold Biotechnology) or DYKDDDDK Fab-trap agarose (ChromoTek) overnight on an end-over-end rotator at 4 °C, washed six times with EBC or RIPA buffer, and resuspended in 2×Laemmli sample buffer. For p97, VCF1 or p47 pulldowns, antibodies (0.5 µg/sample) were coupled to agarose beads, incubated with recombinant proteins or cell lysates and washed with the indicated buffer. To assess p97-UFD1-NPL4 binding to ubiquitylated proteins in total cell extracts, U2OS cells were lysed in EBC buffer supplemented with protease and phosphatase inhibitors, sonicated and incubated on ice for 10 min. Lysates were cleared by centrifugation for 10 min at 20,000 rpm. Cell lysate (40 µg) was added to recombinant proteins in EBC buffer, incubated overnight on the rotator with DYKDDDDK Fab-trap agarose (ChromoTek), and beads were washed six times.

bioRxiv preprint doi: https://doi.org/10.1101/2023.07.25.550448; this version posted July 25, 2023. The copyright holder for this preprint (which was not certified by peer review) is the author/funder, who has granted bioRxiv a license to display the preprint in perpetuity. It is made available under aCC-BY-NC-ND 4.0 International license.

Peptide pulldowns were performed using Streptavidin High Performance beads (GE Healthcare) and either RIPA or EBC buffer. Peptides containing an N-terminal biotin tag were purchased from GenScript and dissolved according to manufacturer's recommendation. The following peptides were used: VCF1-1 (amino acids (aa) 1-46 of human VCF1): MGGRGADAGSSGGTGPTEGYSPPAASTRAAARAKARGGGRG; VCF1-2 (aa24-70): AASTRAAARAKARGGGRGGRRNTTPSVPSLRGAAPRSFHPPAAMSER; VCF1-3 (aa51-99): PSLRGAAPRSFHPPAAMSERLRPRKRRRNGNEEDNHLPPQTKRSSRNPV; VCF1-4 (aa87-128): LPPQTKRSSRNPVFQDSWDTESSGSDSGGSSSSSSSSINSPD; VCF1-5 (aa116-157): SSSSSSSSINSPDRASGPEGSLSQTMAGSSPNTPQPVPEQSA; VCF1-6 (aa145-186): SLSQTMAGSSPNTPQPVPEQSALCQGLYFHINQTLREAHFHSLQHRGRPLT; VIM (SVIP, aa14-39): PTPDLEEKRAKLAEAAERRQKEAAS; VBM (ATXN3, aa275-295): NLTSEELRKRREAYFEKQQQK.

Beads were coupled to peptides for a minimum of 2 h at 4 °C with rotation, blocked in BSA (New England Biolabs) and washed three times for 1 min at 6000 rpm, before incubation overnight at 4 °C with whole cell lysate or purified proteins. Beads were then washed three times for 1 min at 6000 rpm and bound material was eluted in 2×Laemmli sample buffer and analyzed by immunoblotting.

Affinity purification and mass spectrometry

GFP-Trap agarose (Chromotek) pulldowns were subjected to partial on-bead digestion for peptide elution, by addition of 100 µl of elution buffer (50 mM Tris, pH 7.5; 2 M urea; 2 mM DTT; 20 µg/ml trypsin) and incubation at 37 °C for 30 min. To carry out alkylation, 25 mM CAA was added to the samples, which were then left to digest overnight at room temperature.

bioRxiv preprint doi: https://doi.org/10.1101/2023.07.25.550448; this version posted July 25, 2023. The copyright holder for this preprint (which was not certified by peer review) is the author/funder, who has granted bioRxiv a license to display the preprint in perpetuity. It is made available under aCC-BY-NC-ND 4.0 International license.

Digestion was halted by introducing 1% TFA. Purification and desalting of peptides were done using SDB-RPS StageTips. This process required preparing two layers of SDB-RPS with 100 µl of wash buffer (0.2% TFA in H_2O), onto which the peptides were loaded. After centrifugation for 5 min at 500 g, peptides were washed using 150 µl wash buffer, eluted with 50 µl elution buffer (80% ACN; 1 % ammonia) and vacuum-dried.

Liquid chromatography-mass spectrometry (LC-MS) analysis was conducted using an EASY-nLC-1200 system (Thermo Fisher Scientific), coupled with a timsTOF Pro spectrometer and a nano-electrospray ion source (Bruker Daltonik). Peptides were loaded onto a 50 cm custom-packed HPLC-column (75 µm inner diameter filled with 1.9 µm ReproSilPur C18-AQ silica beads, Dr. Maisch). To separate peptides, we followed a linear gradient from 5% to 30% buffer B in 43 min, which then increased to 60% for 7 min, 95% for 5 min, and 5% for a final 5 min at a flow rate of 300 nL/min. Buffer B was a mix of 0.1% formic acid and 80% ACN in LC-MS grade water, while buffer A contained only 0.1% formic acid in LC-MS grade water. The whole gradient cycle lasted for 60 min, and a column oven maintained the column temperature at 60 °C.

Mass spectrometric analysis was carried out in data-dependent (ddaPASEF) mode, as described in [46]. Each cycle incorporated one MS1 survey TIMS-MS and ten PASEF MS/MS scans. Both ion accumulation and ramp time in the dual TIMS analyzer were set to 100 ms. Ion mobility range from 1/K0 = 1.6 Vs/cm^{-2} to 0.6 Vs/cm^{-2} was studied.

Precursor ions for MS/MS analysis were isolated using a 2 Th window for $m/z < 700$ and 3 Th for $m/z > 700$, within an m/z range of 100-1.700. Synchronization of the quadrupole switching events was done according to the precursor elution profile of the TIMS device. The collision energy decreased linearly, starting from 59 eV at 1/K0 = 1.6 VS/cm^{-2} to 20 eV at 1/K0 = 0.6 Vs/cm^{-2}, corresponding to the rise in mobility. We applied a polygon filter (out of control, Bruker Daltonik) to exclude singly charged precursor ions. Precursors for MS/MS

bioRxiv preprint doi: https://doi.org/10.1101/2023.07.25.550448; this version posted July 25, 2023. The copyright holder for this preprint (which was not certified by peer review) is the author/funder, who has granted bioRxiv a license to display the preprint in perpetuity. It is made available under aCC-BY-NC-ND 4.0 International license.

were chosen above an intensity threshold of 1.000 arbitrary units (a.u.) and underwent resequencing until hitting a 'target value' of 20.000 a.u, considering a dynamic exclusion of 40-sec elution.

Crosslinking mass spectrometry

Purified FLAG-p97 and Strep-HA-VCF1 proteins were mixed in 100 µl buffer (30 mM HEPES, pH 7.5; 300 mM NaCl; 1 mM TCEP), with both proteins at a final concentration of 1 µM. To crosslink the proteins, the MS-cleavable crosslinking agent disuccinimidyl dibutyric urea (DSBU) was added to a final concentration of 3 mM, and incubated at 25 °C for 1 h. The crosslinking reaction was stopped by adding Tris-HCl pH 8.0 to a final concentration of 50 mM and incubating at 25 °C for 30 min. Crosslinked proteins were precipitated with four volumes of ice-cold (−20 °C) acetone, and incubated at −20 °C overnight, after which samples were centrifuged at 15,000 rpm for 5 min. The supernatant was removed and the pellet was dried by exposing the pellet to air at room temperature for a few minutes until it started to appear transparent. Protein pellets obtained from acetone precipitation were dissolved and denatured in 25 µl of denaturation-reduction solution (8 M urea; 5 mM TCEP) at 25 °C for 30 min. Alkylation of cysteine residues was performed by adding 2-chloroacetamide (CAA) to a final concentration of 5 mM and incubating at 25 °C for 20 min, after which 25 µl ABC buffer (20 mM ammonium bicarbonate, pH 8.0) was added to reduce the concentration of urea to 4 M. Lys-C digestion (1:200 w/w) was performed at 25 °C for 3 h, followed by trypsin digestion (1:50 w/w) at 25 °C overnight. Urea was diluted to a final concentration of 0.8 M urea using ABC buffer, after which the samples were further digested with Glu-C (1:200 w/w) at 25 °C overnight.

Peptides were purified using StageTips at high pH as described previously [47]. Quad-layer StageTips were prepared using four punch-outs of C18 material (Sigma-Aldrich, Empore SPE Disks, C18, 47 mm). StageTips were equilibrated using 100 µl of methanol, 100 µl of 80

bioRxiv preprint doi: https://doi.org/10.1101/2023.07.25.550448; this version posted July 25, 2023. The copyright holder for this preprint (which was not certified by peer review) is the author/funder, who has granted bioRxiv a license to display the preprint in perpetuity. It is made available under aCC-BY-NC-ND 4.0 International license.

% ACN in 200 mM ammonium hydroxide, and two times 75 µl 50 mM ammonium. Samples were supplemented with one fifth volume of 200 mM ammonium hydroxide (pH >10), just prior to loading them on StageTips. The StageTips were subsequently washed twice with 150 µl 50 mM ammonium hydroxide, and afterwards eluted using 80 µl of 25 % ACN in 50 mM ammonium hydroxide. All samples were dried to completion in protein-LoBind tubes (Eppendorf), using a SpeedVac for 2 h at 60°C, after which the dried peptides were dissolved using 10 µl of 0.1 % formic acid, and stored at −20 °C until MS analysis.

Samples were analyzed on an EASY-nLC 1200 system (Thermo) coupled to an Orbitrap Exploris 480 mass spectrometer (Thermo). Separation of peptides was performed using 20-cm columns (75 µm internal diameter) packed in-house with ReproSil-Pur 120 C18-AQ 1.9 µm beads (Dr. Maisch). Elution of peptides from the column was achieved using a gradient ranging from buffer A (0.1 % formic acid) to buffer B (80 % acetonitrile in 0.1 % formic acid), at a flow of 250 nl/min. The gradient length was 80 min per sample, including ramp-up and wash-out, with an analytical gradient of 60 min ranging from 5% B to 38% B. Analytical columns were heated to 40°C using a column oven, and ionization was achieved using a NanoSpray Flex NG ion source. Spray voltage was set to 2 kV, ion transfer tube temperature to 275°C, and RF funnel level to 50%. Full scan (MS1) range was set to 300-1,300 m/z, MS1 resolution to 120,000, MS1 AGC target to “200” (2,000,000 charges), and MS1 maximum injection time to “Auto”. Precursors with charges 3-6 were selected for fragmentation using an isolation width of 1.3 m/z, and fragmented using higher-energy collision dissociation (HCD) with normalized collision energy of 27. Precursors were excluded from re-sequencing by setting a dynamic exclusion of 60 s. MS/MS (MS2) AGC target was set to “200” (200,000 charges), MS2 maximum injection time to “Auto”, MS2 resolution to 45,000, intensity threshold to 230,000 charges per second, and number of dependent scans to 9.

Analysis of proteomic data

bioRxiv preprint doi: https://doi.org/10.1101/2023.07.25.550448; this version posted July 25, 2023. The copyright holder for this preprint (which was not certified by peer review) is the author/funder, who has granted bioRxiv a license to display the preprint in perpetuity. It is made available under aCC-BY-NC-ND 4.0 International license.

For analysis of affinity purification mass spectrometry data, raw files obtained in ddaPASEF mode were analyzed with MaxQuant (version 1.6.17.0) [48]. Searches were conducted on the UniProt database (2019 release, UP000005640_9606), implementing a peptide spectral match (PSM) and protein level FDR of 1%. The search criteria required a minimum of seven amino acids, including N-terminal acetylation and methionine oxidation as variable modifications, and cysteine carbamidomethylation as a fixed modification. Enzyme specificity was set to trypsin, permitting a maximum of two missed cleavages. The initial and primary search mass tolerance were set to 70 ppm and 20 ppm, respectively. The identification of peptides was accomplished by aligning four-dimensional isotope patterns between the different runs (MBR), utilizing a 0.7-min window for matching retention time and a 0.05 1/K0 window for ion mobility. For label-free quantification, we used the MaxLFQ algorithm [49] with a minimum ratio count of two. Proteomics data were analyzed using Perseus (version 1.6.15.0) [50], and MaxQuant output tables were cleansed of 'Reverse', 'Only identified by site modification', and 'Potential contaminants' entries before the analysis. Missing data was filled in following a meticulous filtering process, based on a standard distribution (width=0.3; downshift=1.8) before performing statistical evaluations. In conducting pairwise comparisons of the proteomics data via a two-sided unpaired t-test, we incorporated a 1 or 5 % permutation-based FDR to account for multiple hypothesis testing, also including an s0 value [51] of 1 or 2.

For analysis of crosslinking mass spectrometry data, the data were first converted from the Thermo-Finnigan RAW format to Mascot Generic Format (MGF) using pFind Studio version 3.1.0 [52]. For this purpose, the RAW files were loaded into pFind, and processed using default data extraction settings and output to MGF enabled. After the pParse and pXtract modules finished the conversion from RAW to MGF, the search in pFind was aborted. To identify DSBU-crosslinked peptides, the MGF files were analyzed using MeroX version 2.0.1.4 [53].

bioRxiv preprint doi: https://doi.org/10.1101/2023.07.25.550448; this version posted July 25, 2023. The copyright holder for this preprint (which was not certified by peer review) is the author/funder, who has granted bioRxiv a license to display the preprint in perpetuity. It is made available under aCC-BY-NC-ND 4.0 International license.

The full-length sequences of human p97 (UniProt: P55072) and VCF1 (UniProt: Q969W3) were used for the search. MeroX default settings were used, with exceptions specified below. Digestion specificity was set to C-terminal of arginine with a maximum of 2 missed cleavages, C-terminal of lysine with a maximum of 2 missed cleavages, C-terminal of glutamic acid with a maximum of 2 missed cleavages, and C-terminal of aspartic acid with a maximum of 4 missed cleavages. The global maximum number of missed cleavages increased to 6, to accommodate low off-target activity of Glu-C towards aspartic acid residues. DSBU crosslinking was set to allow KSTY (site 1) to KSTY (site 2) crosslinks. Analysis mode was set to Quadratic (as intended for 1−10 proteins), and minimum score for individual peptides (in quadratic mode) was increased to 5. Processed data was exported to xiViewer format and visualized online using xiView [54].

Structural modeling of p97 complexes

Structures of complexes between monomeric p97 and human VCF1, SVIP, ATX3, NPL4 and UFD1 were predicted with AlphaFold multimer (version 2.3.1) [26,27] based on full-length amino acid sequences from UniProt. Buried surface areas were calculated with PDBePISA (http://www.ebi.ac.uk/msd-srv/prot_int/picite.html). Structures were visualized in PyMOL (version 1.2r3pre, Schrödinger, LLC).

Surface Plasmon Resonance (SPR)

All SPR experiments were performed at 25 °C on a Biacore T200 instrument equipped with CM5 or CM7 sensor chips (Cytiva, Uppsala, Sweden). SPR running buffers and amine-coupling reagents (N-ethyl-N'-(3-dimethlyaminoproply)carbodiimide (EDC), N-hydroxysuccinimide (NHS), and ethanolamine HCl) were purchased from Cytiva. 1x PBS-P (11.9 mM NaH_2PO_4-Na_2HPO_4, pH 7.4; 137 mM NaCl; 2.7 mM KCl; 0.005% surfactant P20) supplemented with 0.5 mM TCEP was used as running buffer for the immobilization and the binding experiments with Strep-HA-VCF1 full-length proteins. For the VCF1 C-terminal

bioRxiv preprint doi: https://doi.org/10.1101/2023.07.25.550448; this version posted July 25, 2023. The copyright holder for this preprint (which was not certified by peer review) is the author/funder, who has granted bioRxiv a license to display the preprint in perpetuity. It is made available under aCC-BY-NC-ND 4.0 International license.

peptide binding studies, 2% DMSO was additionally included in the running buffer. Eight solvent correction samples ranging from 1.5% DMSO to 2.8% DMSO prepared in either PBS-P, 0.5 mM TCEP or Tris-based buffer were used to correct buffer/DMSO mismatches. The CM5 chip was used for the kinetic analysis of the interactions between p97 proteins and VCF1 full-length proteins or VCF1 C-terminal peptides. p97 was immobilized at different densities on the carboxymethyl dextran sensor chip surface by amine-coupling chemistry. For kinetic analysis, p97 was immobilized at low density (~ 400 RU) on flow cells 2 (Fc2) and 3 (Fc3), respectively, of a CM5 chip. The flow cell 1 (Fc1) remained unmodified and was used as a reference cell for subtraction of systematic instrumental drift. The carboxyl groups were activated for 7 min using 0.1 M NHS and 0.4 M EDC mixed at a 1:1 ratio and a flow rate of 10 µl/min. Short pulses of p97 at 40 µg/ml in 10 mM sodium acetate (pH 5.0) were then flowed over the activated surface until the appropriate immobilization level was reached. The excess activated carboxyl groups were blocked with 1 M ethanolamine, pH 8.5 (7 min injection at a 10 µl/min flow rate). VCF1 C-terminal peptide stocks (150 µM) were prepared in pure DMSO (Sigma Aldrich). Threefold serial dilutions of VCF1 proteins or peptides were prepared in the SPR running buffer from the primary stocks starting from highest concentration of 300 nM (VCF1 C-terminal peptides) or 100 nM (VCF1 full-length proteins). VCF1 peptides and full-length proteins were injected sequentially over all flow cells at a flow rate of 60 µl/min for 120 s. The dissociation rate of the p97-VCF1 complexes was monitored for 400 s. A series of concentrations (2 or 3) were run in duplicates. The experiments were run at least in duplicates to confirm the reproducibility of the assay. Data processing and kinetic fitting were done using the BiaEvaluation software (version 3.2.1, Cytiva, Uppsala, Sweden). The raw sensorgrams were solvent corrected (when appropriate), double referenced (referring to the subtraction of the data over the reference surface and the average of the buffer injections from the binding responses), and the association and dissociation phases

bioRxiv preprint doi: https://doi.org/10.1101/2023.07.25.550448; this version posted July 25, 2023. The copyright holder for this preprint (which was not certified by peer review) is the author/funder, who has granted bioRxiv a license to display the preprint in perpetuity. It is made available under aCC-BY-NC-ND 4.0 International license.

over all replicates were globally fitted using a 1:1 interaction model yielding single values for the k_a and the k_d. The equilibrium dissociation constant, K_d, is the rate of the k_d over the k_a. Binding experiments were measured in triplicates. Data processing and fitting was done using the BiaEvaluation software (version 3.2.1, Cytiva, Uppsala, Sweden). Sensorgrams were solvent corrected and double referenced. The equilibrium dissociation contants, K_d, were determined by plotting the equilibrium responses levels (Req) against nucleotide concentrations and fitting to a steady-state model.

Mass photometry

Mass photometry experiments were performed on a Refeyn One (Refeyn Ltd) mass photometer at room temperature. Measurements were run in triplicates, diluting 3 µl of protein sample (20 nM) in 15 µl PBS buffer loaded on a gasket (Grace Bio-Labs reusable CultureWell gaskets (GBL103250, Merck)) mounted on a glass microscope coverslip (0107222, Marienfeld). Experiments were performed with His_6-p97 alone and in presence of saturating concentrations of full-length Strep-HA-VCF1. The molecular weight was obtained by contrast comparison with known molecular weight mass standard calibrants (NativeMark Unstained Protein Standard (LC0725), Thermo Fischer Scientific) measured on the same buffer and on the same day. Movies were recorded using AcquireMP (Refeyn Ltd, version 2022 R1), with a medium field of view and exposure time of 0.95 ms for the acquisition camera settings. A total of 6000 frames were recorded over a duration of one minute. Movies were processed and analysed with the DiscoverMP software (Refeyn Ltd, version 2022 R1) provided by the instrument manufacturer.

Analytical gel filtration

For analytical gel filtration, p97 alone (5 µM hexamer), or p97 (5 µM hexamer) with UFD1-NPL4 (5 µM) and VCF1 (5 µM) were mixed in a total volume of 25 µl in SEC buffer (50 mM HEPES, pH 7.4; 150 mM NaCl). Samples were separated by size exclusion

bioRxiv preprint doi: https://doi.org/10.1101/2023.07.25.550448; this version posted July 25, 2023. The copyright holder for this preprint (which was not certified by peer review) is the author/funder, who has granted bioRxiv a license to display the preprint in perpetuity. It is made available under aCC-BY-NC-ND 4.0 International license.

chromatography on a Superose 6 3.2/300 column (Cytiva) equilibrated in SEC buffer using an ÄKTA Purifier 10 FPLC system (GE Healthcare). After the column dead volume (0.35 column volumes), fractions were collected (120 µl) and analyzed by immunoblotting.

ATPase assays

For ATPase assays, 1 ml of 5x assay buffer (250 mM Tris, pH 7.4; 100 mM $MgCl_2$; 5 mM EDTA) was mixed with 3 ml water, 5 µl 0.5 M TCEP and 5 µl 10% Triton X. To 40 ul of this assay buffer, recombinant proteins were added, mixed and incubated for 30 min. Final protein concentrations were as follows: p97 (25 nM), VCF1 (range of 0, 0.025, 1, 10 and 25 nM). The reactions were started by adding 10 µl ATP (final concentration of 375 µM) to the 40 µl reactions in a 96 well plate. After 35 min at room temperature, reactions were stopped by adding 50 µl BIOMOL Green reagent (Enzo Life Sciences). Absorbance at 635 nm was measured after 4 min and the relative ATPase activity calculated. Reactions were performed in duplicates and repeated three times.

Acknowledgements

We thank Olaf Stemmann for providing reagents, Satya Pentakota and Dandan Xue for technical support with protein production and AlphaFold applications, respectively, and members of the Mailand laboratory for helpful discussions. This work was supported by grants from Novo Nordisk Foundation (grants no. NNF14CC0001 and NNF18OC0030752), European Union's Horizon 2020 research and innovation program (Marie-Skłodowska-Curie grant agreement no. 812829 (aDDRess) and European Research Council (ERC) grant agreement no. 715975), Lundbeck Foundation (grant no. R223-2016-281), Danish Cancer Society, Independent Research Fund Denmark (grant no. 0134-00048B), and Danish National

bioRxiv preprint doi: https://doi.org/10.1101/2023.07.25.550448; this version posted July 25, 2023. The copyright holder for this preprint (which was not certified by peer review) is the author/funder, who has granted bioRxiv a license to display the preprint in perpetuity. It is made available under aCC-BY-NC-ND 4.0 International license.

Research Foundation (grant no. DNRF-115), German Research Foundation (DFG; SFB1430; Project-ID 424228829) and EMBO (ALTF 1149-2020).

Author Contributions

Conceptualization: A.S.M. and N.M.; Methodology: A.S.M., S.H., M.W., A.M., B.L.M., I.A.H., G.M. and N.M.; Investigation: A.S.M., S.H., M.W., A.M., B.L.M., D.T., J.v.d.B., B.B. and I.A.H.; Writing – Original Draft: N.M.; Writing – Review and Editing: All authors; Supervision, M.L.N., J.P.D., H.M., G.M. and N.M.; Project Administration: N.M.; Funding Acquisition: S.H., B.B., H.M., J.P.D. and N.M.

Conflict of Interest

The authors declare no competing interests.

bioRxiv preprint doi: https://doi.org/10.1101/2023.07.25.550448; this version posted July 25, 2023. The copyright holder for this preprint (which was not certified by peer review) is the author/funder, who has granted bioRxiv a license to display the preprint in perpetuity. It is made available under aCC-BY-NC-ND 4.0 International license.

References

1. van den Boom, J. & Meyer, H. VCP/p97-Mediated Unfolding as a Principle in Protein Homeostasis and Signaling. *Mol Cell* **69**, 182-194 (2018).
2. Ye, Y., Tang, W.K., Zhang, T. & Xia, D. A Mighty "Protein Extractor" of the Cell: Structure and Function of the p97/CDC48 ATPase. *Front Mol Biosci* **4**, 39 (2017).
3. Twomey, E.C. et al. Substrate processing by the Cdc48 ATPase complex is initiated by ubiquitin unfolding. *Science* **365**(2019).
4. Bodnar, N.O. & Rapoport, T.A. Molecular Mechanism of Substrate Processing by the Cdc48 ATPase Complex. *Cell* **169**, 722-735 e9 (2017).
5. Weith, M. et al. Ubiquitin-Independent Disassembly by a p97 AAA-ATPase Complex Drives PP1 Holoenzyme Formation. *Mol Cell* **72**, 766-777 e6 (2018).
6. Cooney, I. et al. Structure of the Cdc48 segregase in the act of unfolding an authentic substrate. *Science* **365**, 502-505 (2019).
7. Pan, M. et al. Mechanistic insight into substrate processing and allosteric inhibition of human p97. *Nat Struct Mol Biol* **28**, 614-625 (2021).
8. Pfeffer, G. et al. Multisystem Proteinopathy Due to VCP Mutations: A Review of Clinical Heterogeneity and Genetic Diagnosis. *Genes (Basel)* **13**(2022).
9. Kilgas, S. & Ramadan, K. Inhibitors of the ATPase p97/VCP: From basic research to clinical applications. *Cell Chem Biol* **30**, 3-21 (2023).
10. Buchberger, A., Schindelin, H. & Hanzelmann, P. Control of p97 function by cofactor binding. *FEBS Lett* **589**, 2578-89 (2015).
11. Stach, L. & Freemont, P.S. The AAA+ ATPase p97, a cellular multitool. *Biochem J* **474**, 2953-2976 (2017).
12. Hanzelmann, P. & Schindelin, H. The Interplay of Cofactor Interactions and Post-translational Modifications in the Regulation of the AAA+ ATPase p97. *Front Mol Biosci* **4**, 21 (2017).
13. Tsuchiya, H. et al. In Vivo Ubiquitin Linkage-type Analysis Reveals that the Cdc48-Rad23/Dsk2 Axis Contributes to K48-Linked Chain Specificity of the Proteasome. *Mol Cell* **66**, 488-502 e7 (2017).
14. Xue, L. et al. Valosin-containing protein (VCP)-Adaptor Interactions are Exceptionally Dynamic and Subject to Differential Modulation by a VCP Inhibitor. *Mol Cell Proteomics* **15**, 2970-86 (2016).
15. Meyer, H. & van den Boom, J. Targeting of client proteins to the VCP/p97/Cdc48 unfolding machine. *Front Mol Biosci* **10**, 1142989 (2023).
16. Ji, Z. et al. Translocation of polyubiquitinated protein substrates by the hexameric Cdc48 ATPase. *Mol Cell* **82**, 570-584 e8 (2022).
17. Williams, C., Dong, K.C., Arkinson, C. & Martin, A. The Ufd1 cofactor determines the linkage specificity of polyubiquitin chain engagement by the AAA+ ATPase Cdc48. *Mol Cell* **83**, 759-769 e7 (2023).
18. Kochenova, O.V., Mukkavalli, S., Raman, M. & Walter, J.C. Cooperative assembly of p97 complexes involved in replication termination. *Nat Commun* **13**, 6591 (2022).
19. Fujisawa, R., Polo Rivera, C. & Labib, K.P.M. Multiple UBX proteins reduce the ubiquitin threshold of the mammalian p97-UFD1-NPL4 unfoldase. *Elife* **11**(2022).
20. Huttlin, E.L. et al. Architecture of the human interactome defines protein communities and disease networks. *Nature* **545**, 505-509 (2017).

bioRxiv preprint doi: https://doi.org/10.1101/2023.07.25.550448; this version posted July 25, 2023. The copyright holder for this preprint (which was not certified by peer review) is the author/funder, who has granted bioRxiv a license to display the preprint in perpetuity. It is made available under aCC-BY-NC-ND 4.0 International license.

21. Raman, M. et al. Systematic proteomics of the VCP-UBXD adaptor network identifies a role for UBXN10 in regulating ciliogenesis. *Nat Cell Biol* **17**, 1356-69 (2015).
22. Hanzelmann, P. & Schindelin, H. The structural and functional basis of the p97/valosin-containing protein (VCP)-interacting motif (VIM): mutually exclusive binding of cofactors to the N-terminal domain of p97. *J Biol Chem* **286**, 38679-38690 (2011).
23. Hanzelmann, P., Buchberger, A. & Schindelin, H. Hierarchical binding of cofactors to the AAA ATPase p97. *Structure* **19**, 833-43 (2011).
24. Beuron, F. et al. Conformational changes in the AAA ATPase p97-p47 adaptor complex. *EMBO J* **25**, 1967-76 (2006).
25. Conicella, A.E. et al. An intrinsically disordered motif regulates the interaction between the p47 adaptor and the p97 AAA+ ATPase. *Proc Natl Acad Sci U S A* **117**, 26226-26236 (2020).
26. Jumper, J. et al. Highly accurate protein structure prediction with AlphaFold. *Nature* **596**, 583-589 (2021).
27. Evans, R. et al. Protein complex prediction with AlphaFold-Multimer. *bioRxiv*, 2021.10.04.463034 (2022).
28. Stapf, C., Cartwright, E., Bycroft, M., Hofmann, K. & Buchberger, A. The general definition of the p97/valosin-containing protein (VCP)-interacting motif (VIM) delineates a new family of p97 cofactors. *J Biol Chem* **286**, 38670-38678 (2011).
29. Isaacson, R.L. et al. Detailed structural insights into the p97-Npl4-Ufd1 interface. *J Biol Chem* **282**, 21361-9 (2007).
30. Lee, H.G., Lemmon, A.A. & Lima, C.D. SUMO enhances unfolding of SUMO-polyubiquitin-modified substrates by the Ufd1/Npl4/Cdc48 complex. *Proc Natl Acad Sci U S A* **120**, e2213703120 (2023).
31. Nguyen, T.Q. et al. Structural basis for the interaction between human Npl4 and Npl4-binding motif of human Ufd1. *Structure* **30**, 1530-1537 e3 (2022).
32. Bekker-Jensen, D.B. et al. An Optimized Shotgun Strategy for the Rapid Generation of Comprehensive Human Proteomes. *Cell Syst* **4**, 587-599 e4 (2017).
33. Dantuma, N.P., Lindsten, K., Glas, R., Jellne, M. & Masucci, M.G. Short-lived green fluorescent proteins for quantifying ubiquitin/proteasome-dependent proteolysis in living cells. *Nat Biotechnol* **18**, 538-43 (2000).
34. Beskow, A. et al. A conserved unfoldase activity for the p97 AAA-ATPase in proteasomal degradation. *J Mol Biol* **394**, 732-46 (2009).
35. Chou, T.F. & Deshaies, R.J. Quantitative cell-based protein degradation assays to identify and classify drugs that target the ubiquitin-proteasome system. *J Biol Chem* **286**, 16546-54 (2011).
36. Godderz, D. et al. Cdc48-independent proteasomal degradation coincides with a reduced need for ubiquitylation. *Sci Rep* **5**, 7615 (2015).
37. Ye, Y., Meyer, H.H. & Rapoport, T.A. Function of the p97-Ufd1-Npl4 complex in retrotranslocation from the ER to the cytosol: dual recognition of nonubiquitinated polypeptide segments and polyubiquitin chains. *J Cell Biol* **162**, 71-84 (2003).
38. Wang, B. et al. Structure and ubiquitin interactions of the conserved zinc finger domain of Npl4. *J Biol Chem* **278**, 20225-34 (2003).
39. Trusch, F. et al. The N-terminal Region of the Ubiquitin Regulatory X (UBX) Domain-containing Protein 1 (UBXD1) Modulates Interdomain Communication within the Valosin-containing Protein p97. *J Biol Chem* **290**, 29414-27 (2015).

bioRxiv preprint doi: https://doi.org/10.1101/2023.07.25.550448; this version posted July 25, 2023. The copyright holder for this preprint (which was not certified by peer review) is the author/funder, who has granted bioRxiv a license to display the preprint in perpetuity. It is made available under aCC-BY-NC-ND 4.0 International license.

40. Shearer, R.F. et al. K27-linked ubiquitylation promotes p97 substrate processing and is essential for cell proliferation. *EMBO J* **41**, e110145 (2022).
41. Lebofsky, R., Takahashi, T. & Walter, J.C. DNA replication in nucleus-free Xenopus egg extracts. *Methods Mol Biol* **521**, 229-52 (2009).
42. Sparks, J. & Walter, J.C. Extracts for Analysis of DNA Replication in a Nucleus-Free System. *Cold Spring Harb Protoc* **2019**(2019).
43. Heubes, S. & Stemmann, O. The AAA-ATPase p97-Ufd1-Npl4 is required for ERAD but not for spindle disassembly in Xenopus egg extracts. *J Cell Sci* **120**, 1325-9 (2007).
44. Poulsen, M., Lukas, C., Lukas, J., Bekker-Jensen, S. & Mailand, N. Human RNF169 is a negative regulator of the ubiquitin-dependent response to DNA double-strand breaks. *J Cell Biol* **197**, 189-99 (2012).
45. Toledo, L.I. et al. ATR prohibits replication catastrophe by preventing global exhaustion of RPA. *Cell* **155**, 1088-103 (2013).
46. Brunner, A.D. et al. Ultra-high sensitivity mass spectrometry quantifies single-cell proteome changes upon perturbation. *Mol Syst Biol* **18**, e10798 (2022).
47. Hendriks, I.A. et al. Site-specific characterization of endogenous SUMOylation across species and organs. *Nat Commun* **9**, 2456 (2018).
48. Cox, J. & Mann, M. MaxQuant enables high peptide identification rates, individualized p.p.b.-range mass accuracies and proteome-wide protein quantification. *Nat Biotechnol* **26**, 1367-72 (2008).
49. Cox, J. et al. Accurate proteome-wide label-free quantification by delayed normalization and maximal peptide ratio extraction, termed MaxLFQ. *Mol Cell Proteomics* **13**, 2513-26 (2014).
50. Tyanova, S. et al. The Perseus computational platform for comprehensive analysis of (prote)omics data. *Nat Methods* **13**, 731-40 (2016).
51. Tusher, V.G., Tibshirani, R. & Chu, G. Significance analysis of microarrays applied to the ionizing radiation response. *Proc Natl Acad Sci U S A* **98**, 5116-21 (2001).
52. Chi, H. et al. Comprehensive identification of peptides in tandem mass spectra using an efficient open search engine. *Nat Biotechnol* (2018).
53. Iacobucci, C. et al. A cross-linking/mass spectrometry workflow based on MS-cleavable cross-linkers and the MeroX software for studying protein structures and protein-protein interactions. *Nat Protoc* **13**, 2864-2889 (2018).
54. Graham, M., Combe, C., Kolbowski, L. & Rappsilber, J. xiView: A common platform for the downstream analysis of Crosslinking Mass Spectrometry data. *bioRxiv*, 561829 (2019).

bioRxiv preprint doi: https://doi.org/10.1101/2023.07.25.550448; this version posted July 25, 2023. The copyright holder for this preprint (which was not certified by peer review) is the author/funder, who has granted bioRxiv a license to display the preprint in perpetuity. It is made available under aCC-BY-NC-ND 4.0 International license.

Figure legends

Figure 1.

VCF1 is a p97-binding protein that interacts tightly with the p97 N-domain

A. Representative images of U2OS/GFP-VCF1 WT cells treated or not with Doxycycline (DOX) for 16 h. Scale bars, 10 μM.

B. Immunoblot analysis of U2OS/GFP-VCF1 WT cells treated as in (A).

C. Mass spectrometry analysis of VCF1-interacting proteins. U2OS/GFP-VCF1 WT cells were treated or not with DOX for 16 h, subjected to GFP immunoprecipitation (IP) in partially denaturing RIPA buffer and analyzed by mass spectrometry. Volcano plot shows enrichment of individual proteins (+DOX/-DOX ratio) plotted against the *P* value (**Table S1**). Dashed lines indicate the significance thresholds (two-sided *t*-test, FDR<0.05, s_0=1).

D. Immunoblot analysis of VCF1 or pre-immune serum (IgG) IPs from whole cell lysates of U2OS cells transfected with non-targeting control (CTRL) or VCF1 siRNAs. Three specific bands corresponding to different VCF1 isoforms are detected by the VCF1 antibody, with the slower-migrating major band representing the 186-amino acid protein (isoform 1).

E. Immunoblot analysis of *in vitro* binding reactions in RIPA buffer containing purified His_6-p97 and Strep-HA-VCF1 proteins that were subjected to StrepTactin (Strep) pulldown.

F. Schematic showing recombinant His_6-p97 proteins used in (G).

G. As in (E), but using recombinant His_6-p97 proteins shown in (F).

H. Surface Plasmon Resonance (SPR) sensorgrams for the interaction between recombinant Strep-HA-VCF1 WT and immobilized His_6-p97 proteins. For His_6-p97 WT (left panel), black traces represent the experimental data and red traces correspond to the global fit of the two replicates according to a 1:1 interaction model. For the His_6-p97 Y143A mutant (right panel), no dose-dependent response was observed.

bioRxiv preprint doi: https://doi.org/10.1101/2023.07.25.550448; this version posted July 25, 2023. The copyright holder for this preprint (which was not certified by peer review) is the author/funder, who has granted bioRxiv a license to display the preprint in perpetuity. It is made available under aCC-BY-NC-ND 4.0 International license.

Figure 2.

VCF1 binds p97 via a novel α-helical motif (VRM)

A. Schematic of VCF1 peptides used in (B).

B. Biotinylated VCF1 peptides in (A) were incubated with whole cell extracts of U2OS cells, subjected to StrepTactin (Strep) pulldown in RIPA buffer and analyzed by immunoblotting.

C. Immunoblot analysis of GFP IPs from U2OS cells transfected with indicated GFP-VCF1 expression constructs.

D. Sequence alignment showing conservation of the p97-binding motif (VRM) in selected vertebrate VCF1 proteins.

E. Comparison of VCF1 WT and N167A interactomes. U2OS/GFP-VCF1 WT or N167A cells treated with DOX for 16 h were subjected to GFP IP in non-denaturing EBC buffer and analyzed by mass spectrometry. Volcano plot shows enrichment of individual proteins (WT/N167A ratio) plotted against the *P* value (**Table S3**). Dashed lines indicate the significance thresholds (two-sided *t*-test, FDR<0.01, s_0=2).

F. SPR sensorgrams for the interaction between VCF1-6 peptide (A) and immobilized recombinant His_6-p97. For the VCF1-6 WT peptide (left panel), black traces represent the experimental data and red traces correspond to the global fit of the two replicates according to a 1:1 interaction model. For the VCF1-6 N167A peptide (right panel), no dose-dependent response was observed.

Figure 3.

Structural modeling of VCF1-p97 complex formation

A. AlphaFold-Multimer model of the complex between full-length VCF1 and a p97 monomer (colored by domains), predicting that the C-terminus of the otherwise highly unstructured

bioRxiv preprint doi: https://doi.org/10.1101/2023.07.25.550448; this version posted July 25, 2023. The copyright holder for this preprint (which was not certified by peer review) is the author/funder, who has granted bioRxiv a license to display the preprint in perpetuity. It is made available under aCC-BY-NC-ND 4.0 International license.

VCF1 forms an α-helix (pink, residues 158-186) that interacts with the groove of the bipartite p97 N-domain (left panel).

B. Closeup view of the VCF1-p97 binding interface predicted by AlphaFold-Multimer (A), showing that it is involves Y143 (yellow) in the p97 N-domain and residues N167, L170 and H174 (blue) in VCF1 (right panel).

C. Comparison of AlphaFold-Multimer models of the complexes formed between the p97 monomer (N-domain in pale cyan) and VCF1 (pink), SVIP (rosa) or ATXN3 (yellow).

D. Biotinylated peptides spanning the VRM in VCF1, VIM in SVIP or VBM in ATXN3 immobilized on StrepTactin agarose were incubated with purified WT or mutant His_6-p97 proteins, washed extensively in RIPA buffer and analyzed by immunoblotting.

E. Schematic visualization of all heteromeric VCF1-p97 crosslinks identified by mass spectrometry analysis of purified FLAG-p97 and Strep-HA-VCF1 proteins incubated with the crosslinker disuccinimidyl dibutyric urea (DSBU) (**Figure S3F**). Self-crosslinks are not shown. All visualized crosslinks scored >50 using MeroX, with a score of at least 19.4 required to ensure an FDR<0.01 via decoy analysis. The line highlighted in blue visualizes a crosslink (with MeroX score of 116) between the p97 N-domain (K136) and the VCF1 VRM (Y163) (**Figure S3E**).

Figure 4.

VCF1 and UFD1-NPL4 form a joint complex with p97

A. Mass photometry-based mass distribution of His_6-p97 (blue) and His_6-p97 in the presence of saturating concentrations of full-length Strep-HA-VCF1 WT (magenta) (left panel) or N167A mutant (grey) (right panel). The mass photometry measurements show major species with molecular weights of 535 kDa (corresponding to a p97 hexamer) and 591 kDa (corresponding to a p97 hexamer bound by 2-3 VCF1 molecules).

bioRxiv preprint doi: https://doi.org/10.1101/2023.07.25.550448; this version posted July 25, 2023. The copyright holder for this preprint (which was not certified by peer review) is the author/funder, who has granted bioRxiv a license to display the preprint in perpetuity. It is made available under aCC-BY-NC-ND 4.0 International license.

B. Binding reactions containing indicated combinations of purified Strep-HA-VCF1, His_6-p97 and GST-UFD1-NPL4 proteins were subjected to Glutathione (GST) pulldown and analyzed by immunoblotting.

C. As in (B), except reactions containing indicated combinations of purified Strep-HA-VCF1, His_6-p97 and UFD1-His_6-NPL4 proteins were subjected to StrepTactin (Strep) pulldown.

D. Purified VCF1 was incubated alone or with equimolar concentrations of p97 and UFD1-NPL4 and then separated by size-exclusion chromatography (SEC). Immunoblot analysis of indicated fractions shows comigration of the p97-VCF1-UFD1-NPL4 complex.

Figure 5.

VCF1 stimulates p97-UFD1-NPL4 recruitment to ubiquitylated substrates to facilitate their degradation

A. Representative images of U2OS/Ub(G76V)-GFP cells transfected with indicated siRNAs. Scale bar, 10 μM.

B. U2OS/Ub(G76V)-GFP cells transfected with indicated siRNAs were subjected to quantitative image-based cytometry (QIBC) analysis of Ub(G76V)-GFP expression (solid lines, median; dashed lines, quartiles; >10000 cells analyzed per condition).

C. Immunoblot analysis of *in vitro* binding reactions containing indicated combinations of purified FLAG-p97, Strep-HA-VCF1, UFD1-His_6-NPL4 complex and K48-linked ubiquitin chains (K48-Ub_{2-7}) that were subjected to FLAG IP.

D. As in (C), except that *in vitro* binding reactions containing purified proteins were incubated with whole cell extracts of U2OS cells where indicated and subjected to FLAG IP.

E. As in (D), using WT or ubiquitin binding-deficient (*UBD) UFD1-His_6-NPL4 complex.

F. Model of VCF1-dependent stimulation of p97-UFD1-NPL4 binding to ubiquitylated client proteins. See main text for details.

bioRxiv preprint doi: https://doi.org/10.1101/2023.07.25.550448; this version posted July 25, 2023. The copyright holder for this preprint (which was not certified by peer review) is the author/funder, who has granted bioRxiv a license to display the preprint in perpetuity. It is made available under aCC-BY-NC-ND 4.0 International license.

Supplementary Figure S1 (related to Figure 1).

VCF1 is a p97-interacting protein

A. BioPlex interactome (https://bioplex.hms.harvard.edu/) for p97 (VCP) in HEK293T cells [20].

B. Sequence alignment of selected vertebrate VCF1 orthologs, using ClustalOmega.

C. Mass spectrometry analysis of VCF1-interacting proteins. U2OS/GFP-VCF1 WT cells were treated or not with DOX for 16 h, subjected to GFP IP in non-denaturing EBC buffer and analyzed by mass spectrometry. Volcano plot shows enrichment of individual proteins (+DOX/-DOX ratio) plotted against the *P* value (**Table S2**). Dashed lines indicate the significance thresholds (two-sided *t*-test, FDR<0.01, s_0=1).

D. Coomassie Blue staining of His_6-p97 proteins purified from *E. coli* and resolved by SDS-PAGE.

E. Coomassie Blue staining of Strep-HA-VCF1 proteins purified from HEK293-6E cells and resolved by SDS-PAGE.

F. Immunoblot analysis of *Xenopus* egg extracts subjected to IP with the indicated antibodies targeting the N-terminal (VCF1-N) or C-terminal (VCF1-C) region of VCF1, p97, NPL4 or an IgG control.

G. Coomassie Blue staining of full-length and truncated His_6-p97 proteins purified from *E. coli* and resolved by SDS-PAGE.

Supplementary Figure S2 (related to Figure 2).

VCF1 binds p97 via a novel α-helical motif (VRM)

A. AlphaFold2 model of human VCF1.

bioRxiv preprint doi: https://doi.org/10.1101/2023.07.25.550448; this version posted July 25, 2023. The copyright holder for this preprint (which was not certified by peer review) is the author/funder, who has granted bioRxiv a license to display the preprint in perpetuity. It is made available under aCC-BY-NC-ND 4.0 International license.

B. Representative images of U2OS/GFP-VCF1 N167A cells treated or not with Doxycycline (DOX) for 16 h. Scale bars, 10 μM.

C. Immunoblot analysis of U2OS/GFP-VCF1 WT cells treated as in (B).

D. Immunoblot analysis of *in vitro* binding reactions containing purified FLAG-p97 and Strep-HA-VCF1 proteins that were subjected to StrepTactin (Strep) pulldown.

E. SPR sensorgrams for the interaction between recombinant Strep-HA-VCF1 N167A and immobilized His_6-p97 WT. Grey bar denotes the region where the data was averaged to calculate the equilibrium binding responses at each concentration.

Supplementary Figure S3 (related to Figure 3).

Structural modeling of VCF1-p97 complex formation

A. AlphaFold-Multimer prediction of the complex between full-length VCF1 (color-coded by pLDDT value (measure of model confidence)) and a p97 monomer (colored by domains).

B. Comparison of AlphaFold-Multimer models of the complexes formed between the p97 monomer (N-domain in pale cyan) and VCF1 (pink), NPL4 (blue) or UFD1 (green).

C. Immunoblot analysis of *in vitro* binding reactions containing purified His_6-p47 and His_6-p97 proteins that were subjected to IP using pre-immune serum (IgG) or p47 antibody.

D. Surface representation of the structure of the p97 N-domain (pale cyan), based on the p97-VCF1 AlphaFold-Multimer prediction in (A). Colored areas correspond to buried surface area calculated with PDBePISA (https://www.ebi.ac.uk/pdbe/pisa/) based on the p97-VCF1 (pink), p97-SVIP (rosa) and p97-ATXN3 (yellow) AlphaFold-Multimer models (**Figure 3C**). VCF1 covers a larger surface area on the p97 N-domain (~1119 $Å^2$) than SVIP (~758 $Å^2$) and ATXN3 (~739 $Å^2$). Residues predicted to reside at the p97-cofactor interface and used for the buried surface area calculation that are exclusively buried by VCF1, SVIP or ATXN3 are labeled in white, rosa and yellow, respectively. Residues common to the buried surface of all

bioRxiv preprint doi: https://doi.org/10.1101/2023.07.25.550448; this version posted July 25, 2023. The copyright holder for this preprint (which was not certified by peer review) is the author/funder, who has granted bioRxiv a license to display the preprint in perpetuity. It is made available under aCC-BY-NC-ND 4.0 International license.

cofactor complexes are labeled in black, residues shared between VCF1 and ATX3 are labeled in orange, and residues shared between VCF1 and SVIP are labeled in green.

E. Fully annotated MS/MS spectrum demonstrating the DSBU crosslink between K136 in p97 and Y163 in VCF1. Top left; peptide fragment coverage map, with bold lines indicating identified fragments ('cm' indicates the presence of carbamidomethyl on the cysteine residue as a result of sample alkylation). Center; MS/MS spectrum with fragment ions originating from VCF1 in red, and fragment ions originating from p97 in blue ('+P' indicates fragment ions including the DSBU crosslink). Top right; fragment mass error in relation to fragment abundance in the MS/MS spectrum, with a maximum error tolerance of 10 ppm.

F. Coomassie Blue staining of purified FLAG-p97 and Strep-HA-VCF1 proteins incubated in the absence or presence of the crosslinker disuccinimidyl dibutyric urea (DSBU), demonstrating efficient DSBU-dependent crosslinking between FLAG-p97 hexamers and Strep-HA-VCF1.

Supplementary Figure S4 (related to Figure 4).

VCF1 and other cofactors form joint complexes with p97

A. Coomassie Blue staining of GST-UFD1-NPL4 complex purified from *E. coli* and resolved by SDS-PAGE.

B. Binding reactions containing indicated combinations of purified Strep-HA-VCF1, His_6-p97 and His_6-p47 proteins were subjected to IP with p47 antibody and analyzed by immunoblotting.

C. Coomassie Blue staining of His_6-p47 purified from *E. coli* and resolved by SDS-PAGE.

D. Binding reactions containing indicated combinations of purified Strep-HA-VCF1, His_6-p97 and FLAG-FAF1 proteins were subjected to FLAG IP and analyzed by immunoblotting.

bioRxiv preprint doi: https://doi.org/10.1101/2023.07.25.550448; this version posted July 25, 2023. The copyright holder for this preprint (which was not certified by peer review) is the author/funder, who has granted bioRxiv a license to display the preprint in perpetuity. It is made available under aCC-BY-NC-ND 4.0 International license.

E. Coomassie Blue staining of FLAG-FAF1 purified from *E. coli* and resolved by SDS-PAGE.

F. Coomassie Blue staining of WT and ubiquitin binding-deficient (*UBD) UFD1-His_6-NPL4 complex purified from *E. coli* and resolved by SDS-PAGE.

G. Immunoblot analysis of U2OS cells transfected with indicated siRNAs and subjected to IP with VCF1 antibody.

H. Composite model of a potential human p97 hexamer bound to a UFD1-NPL4 heterodimer and three copies of the VRM helix, generated by superimposing three copies of the AlphaFold-Multimer prediction of monomeric p97-VRM (**Figure 3A**) onto three p97 subunits within an AlphaFold-Multimer model of the human p97-UFD1-NPL4 complex.

I. Binding reactions containing indicated combinations of purified Strep-HA-VCF1, His_6-p97 and UFD1-His_6-NPL4 proteins were subjected to IP with p97 antibody and analyzed by immunoblotting.

J. Binding reactions containing indicated combinations of purified Strep-HA-VCF1, His_6-p97 and increasing concentrations of His_6-p47 were subjected to StrepTactin (Strep) pulldown and analyzed by immunoblotting.

Supplementary Figure S5 (related to Figure 5).

VCF1 stimulates p97-UFD1-NPL4 recruitment to ubiquitylated substrates to facilitate their degradation

A. Schematic of p97- and/or proteasome-dependent degradation of fluorescent Ub(G76V)-GFP and Ub(G76V)-GFP-20AA reporters.

B. Immunoblot analysis of U2OS/Ub(G76V)-GFP cells in **Figure 5B** transfected with indicated siRNAs.

bioRxiv preprint doi: https://doi.org/10.1101/2023.07.25.550448; this version posted July 25, 2023. The copyright holder for this preprint (which was not certified by peer review) is the author/funder, who has granted bioRxiv a license to display the preprint in perpetuity. It is made available under aCC-BY-NC-ND 4.0 International license.

C. U2OS/Ub(G76V)-GFP-20AA cells were transfected with siRNAs and, where indicated, treated with the proteasome inhibitor MG132 for 2 h prior to fixation. Ub(G76V)-GFP-20AA intensity was analyzed by quantitative image-based cytometry QIBC (solid lines, median; dashed lines, quartiles; >10000 cells analyzed per condition).

D. U2OS/Ub(G76V)-GFP cells transfected with siRNAs were treated with p97 inhibitor (p97i; NMS-873) for 4 h. Cells were then washed thoroughly and collected at the indicated times after p97i withdrawal. Ub(G76V)-GFP intensity was analyzed by QIBC (solid lines, median; dashed lines, quartiles; >10000 cells analyzed per condition).

E. Normalized logarithmic cell proliferation quantification for U2OS cells transfected with indicated siRNAs, determined by Incucyte image-based confluence analysis. Data from a representative experiment are shown.

F. Immunoblot analysis of U2OS cells transfected with indicated siRNAs.

G. U2OS/Ub(G76V)-GFP cells transfected with expression constructs encoding indicated FLAG-tagged plasmids were fixed and immunostained with FLAG antibody. Ub(G76V)-GFP intensity in FLAG-positive cells was analyzed by QIBC (solid lines, median; dashed lines, quartiles; >10000 cells analyzed per condition).

H. Relative ATPase activity of recombinant His_6-p97 protein (25 nM) incubated with indicated concentrations of purified Strep-HA-VCF1 proteins (n=3 independent experiments).

I. Coomassie Blue staining of FLAG-p97 purified from *E. coli* and resolved by SDS-PAGE.

J. *In vitro* binding reactions containing indicated combinations of purified Strep-HA-VCF1 and K48-linked ubiquitin chains (K48-Ub_{2-16}) were subjected to StrepTactin pulldown and analyzed by immunoblotting.

bioRxiv preprint doi: https://doi.org/10.1101/2023.07.25.550448; this version posted July 25, 2023. The copyright holder for this preprint (which was not certified by peer review) is the author/funder, who has granted bioRxiv a license to display the preprint in perpetuity. It is made available under aCC-BY-NC-ND 4.0 International license.

K. Immunoblot analysis of *in vitro* binding reactions containing indicated combinations of purified FLAG-p97, UFD1-His_6-NPL4 complex, whole cell extracts of U2OS cells and full-length or truncated VCF1 proteins that were subjected to FLAG IP.

Supplementary Table S1.

Mass spectrometry analysis of GFP-VCP1 WT IPs in partially denaturing RIPA buffer, related to Figure 1C

Supplementary Table S2.

Mass spectrometry analysis of GFP-VCP1 WT IPs in non-denaturing buffer, related to Figure S1C

Supplementary Table S3.

Mass spectrometry analysis of GFP-VCP1 WT and N167A IPs in partially denaturing RIPA buffer, related to Figure 2E

bioRxiv preprint doi: https://doi.org/10.1101/2023.07.25.550448; this version posted July 25, 2023. The copyright holder for this preprint (which was not certified by peer review) is the author/funder, who has granted bioRxiv a license to display the preprint in perpetuity. It is made available under aCC-BY-NC-ND 4.0 International license.

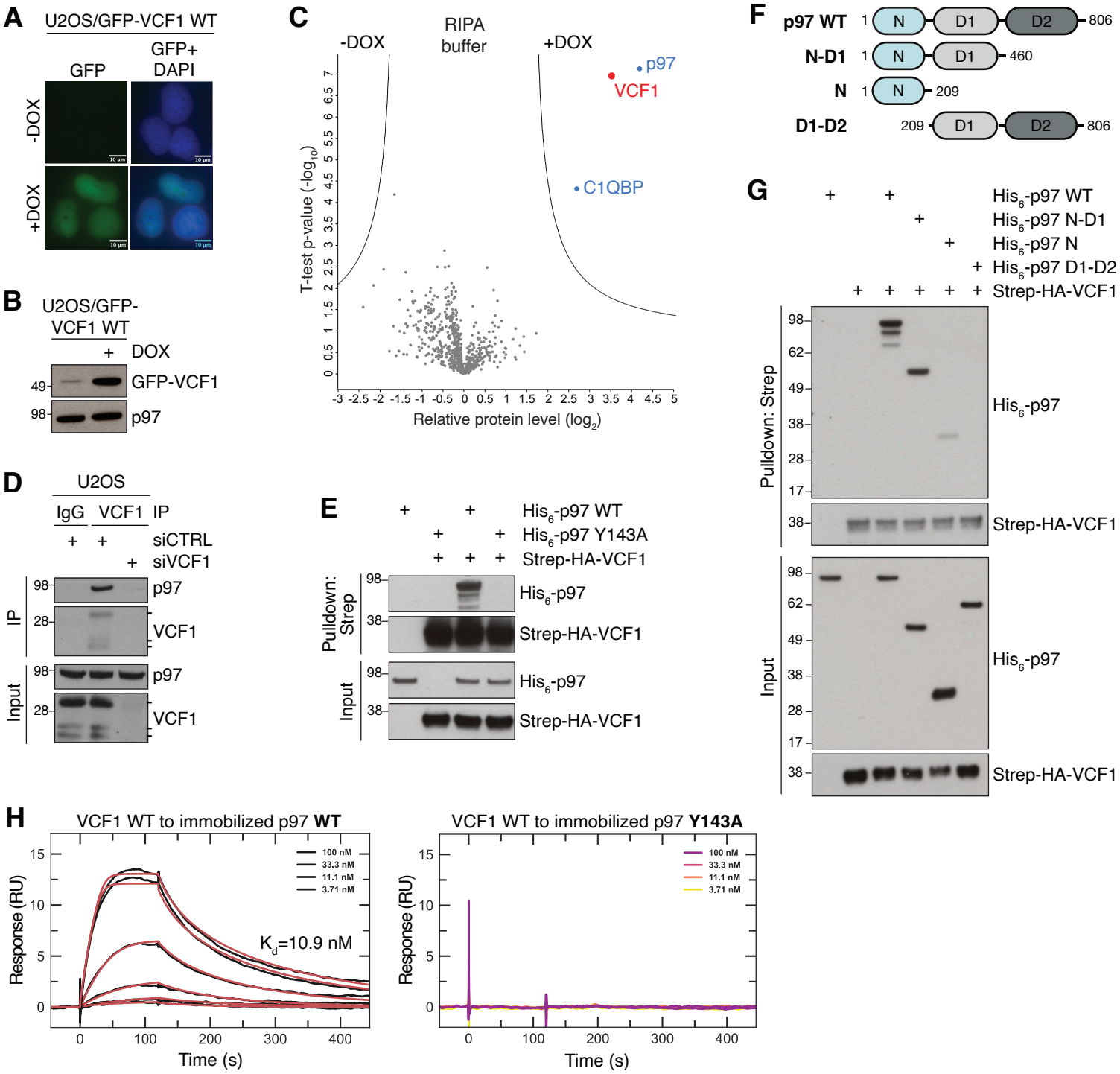

bioRxiv preprint doi: https://doi.org/10.1101/2023.07.25.550448; this version posted July 25, 2023. The copyright holder for this preprint (which was not certified by peer review) is the author/funder, who has granted bioRxiv a license to display the preprint in perpetuity. It is made available under aCC-BY-NC-ND 4.0 International license.

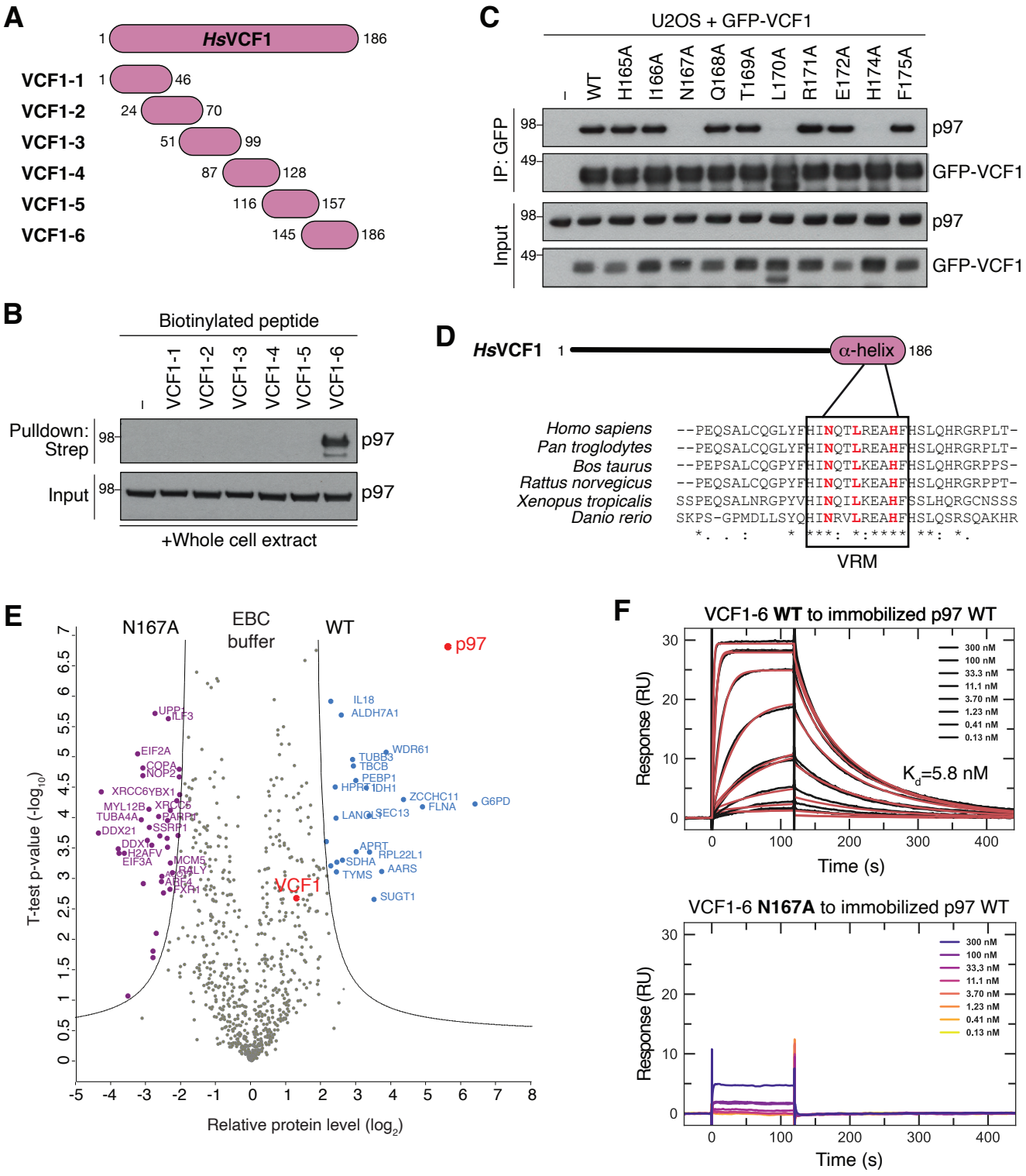

bioRxiv preprint doi: https://doi.org/10.1101/2023.07.25.550448; this version posted July 25, 2023. The copyright holder for this preprint (which was not certified by peer review) is the author/funder, who has granted bioRxiv a license to display the preprint in perpetuity. It is made available under aCC-BY-NC-ND 4.0 International license.

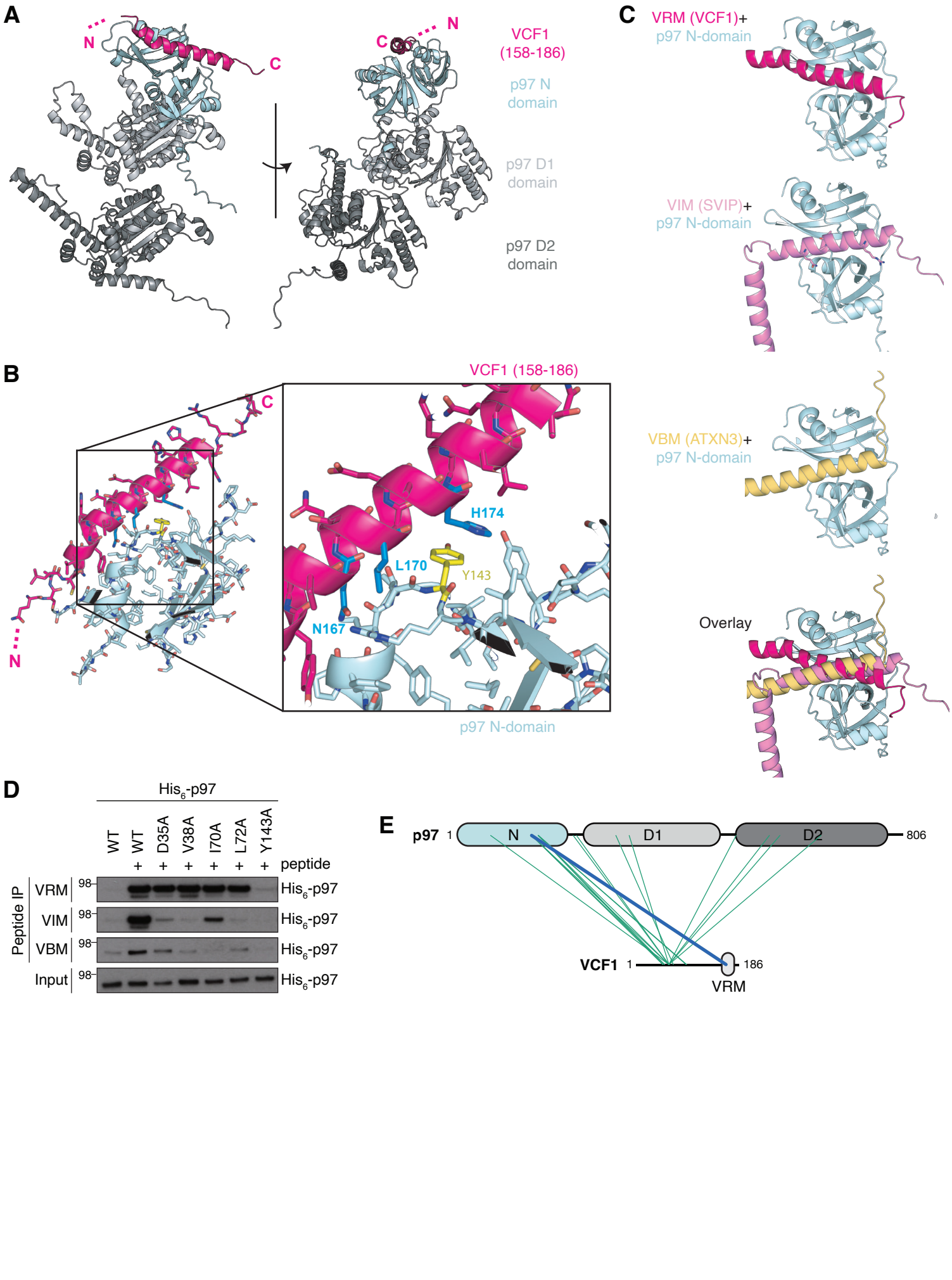

bioRxiv preprint doi: https://doi.org/10.1101/2023.07.25.550448; this version posted July 25, 2023. The copyright holder for this preprint (which was not certified by peer review) is the author/funder, who has granted bioRxiv a license to display the preprint in perpetuity. It is made available under aCC-BY-NC-ND 4.0 International license.

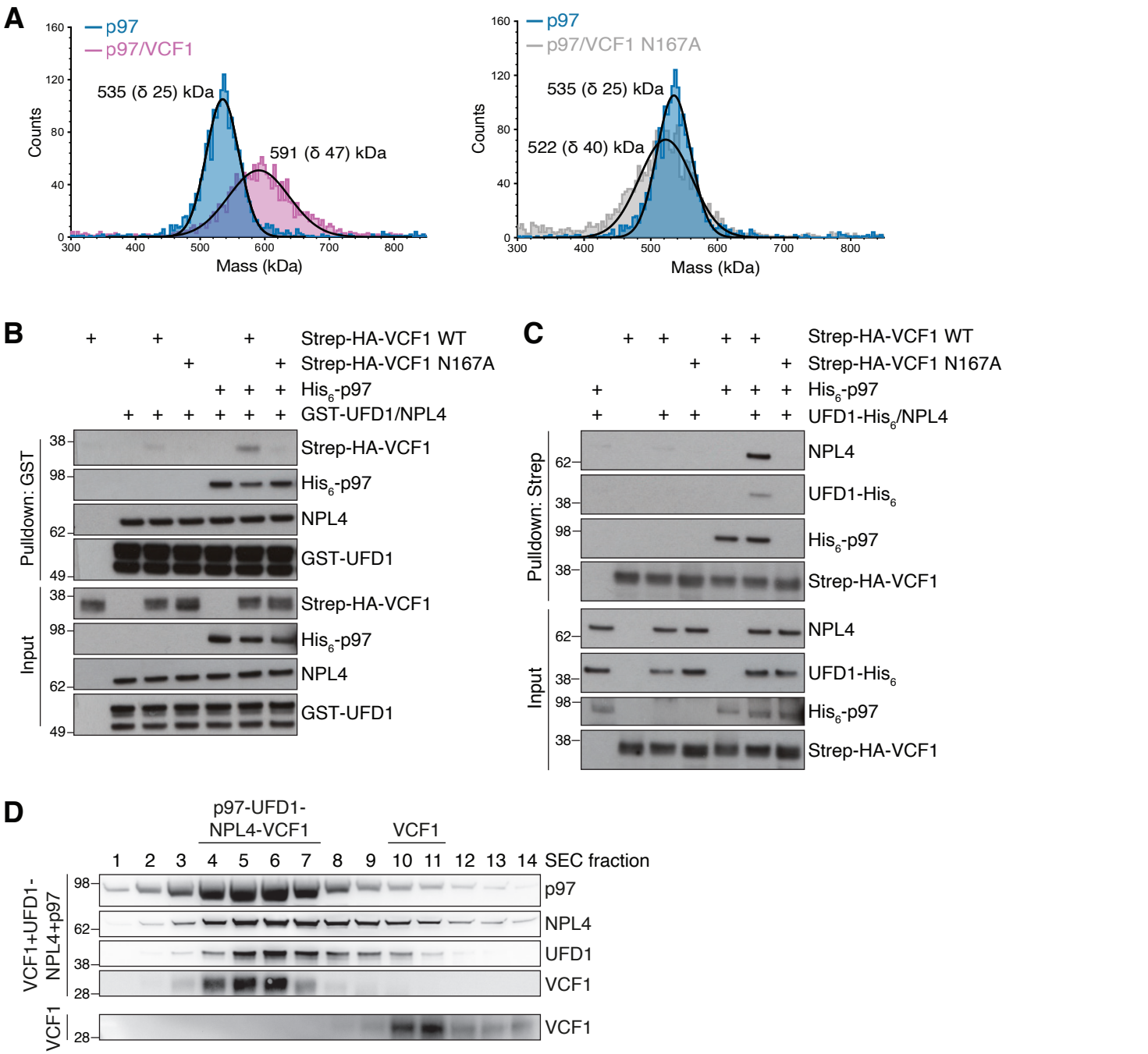

bioRxiv preprint doi: https://doi.org/10.1101/2023.07.25.550448; this version posted July 25, 2023. The copyright holder for this preprint (which was not certified by peer review) is the author/funder, who has granted bioRxiv a license to display the preprint in perpetuity. It is made available under aCC-BY-NC-ND 4.0 International license.

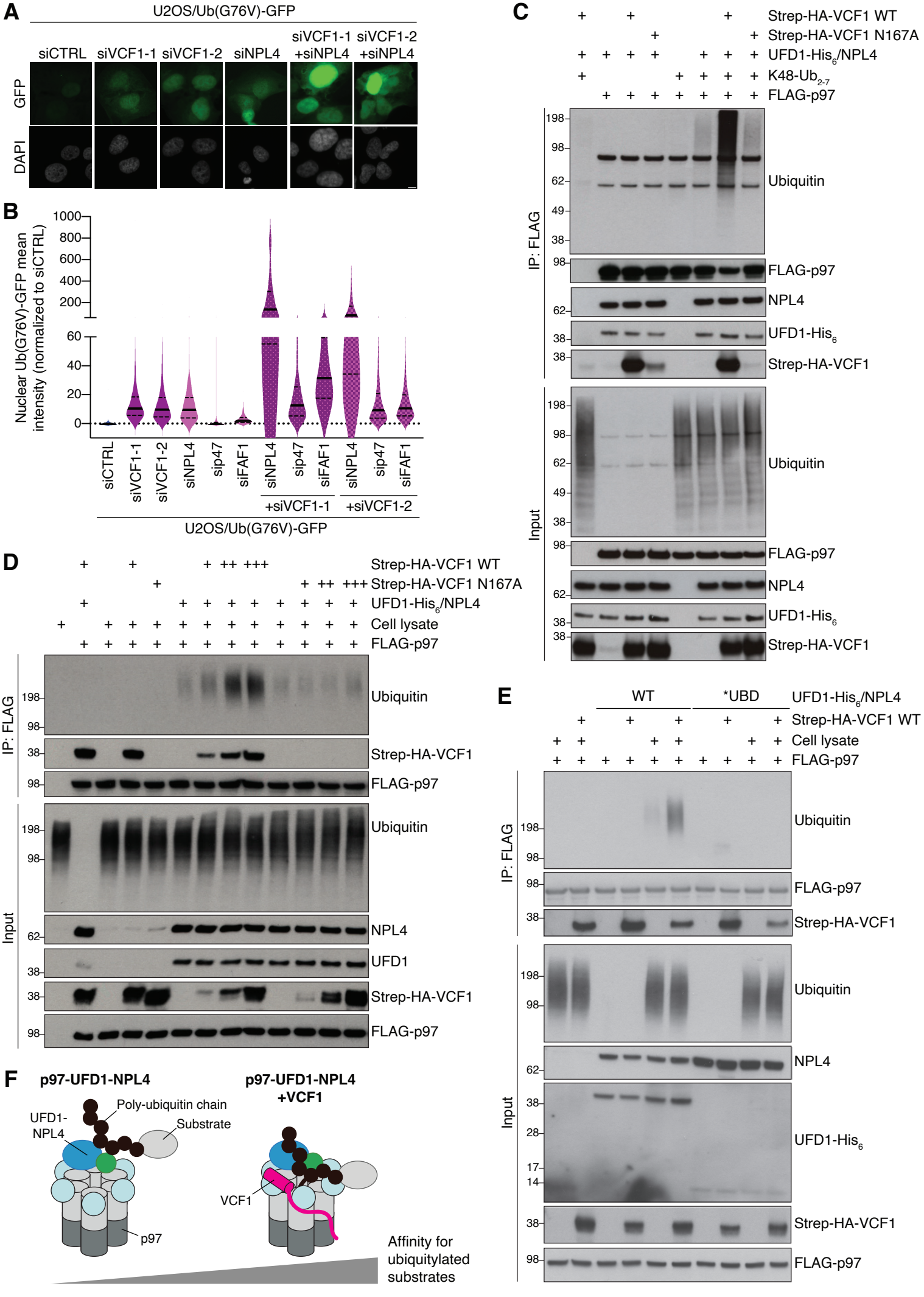

bioRxiv preprint doi: https://doi.org/10.1101/2023.07.25.550448; this version posted July 25, 2023. The copyright holder for this preprint (which was not certified by peer review) is the author/funder, who has granted bioRxiv a license to display the preprint in perpetuity. It is made available under aCC-BY-NC-ND 4.0 International license.

A

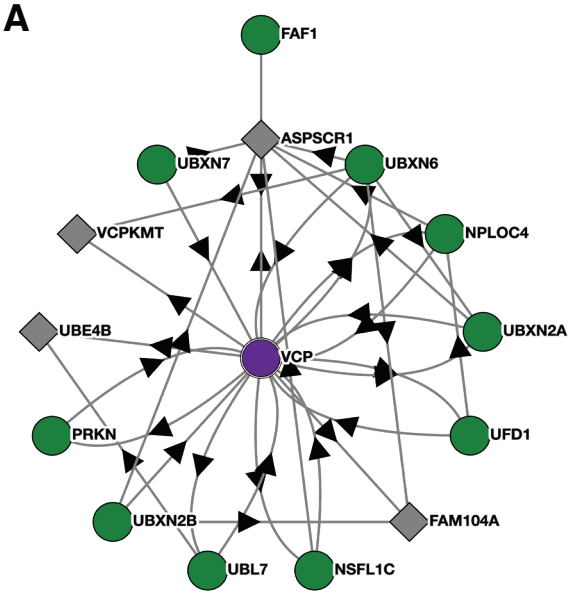

C

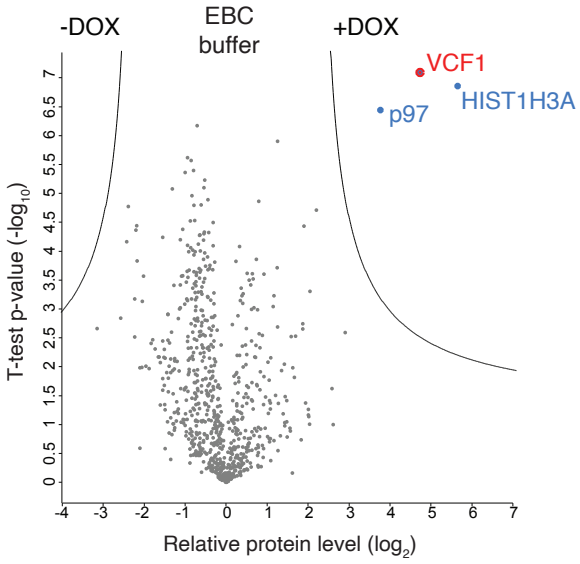

B

```
Homo sapiens          MGGRGADAGSSGGTGPTEGYSPPAASTRAAARAKARGGGRGGRRNTTPSVPSLRGAAPRS  60
Pan troglodytes       ------------------------------------------------------------  0
Bos taurus            MGGRGADAGSSGGTGPPEGYSAPAASARAASRAKARGGGRGGRRNTTPSVPSPRGAAPRR  60
Rattus norvegicus     MGRRGGDTGSSCGTGGTEGYSPPAASTRAAVRAQARGGGRGGRRNTTPTVRCRRGAAPRR  60
Xenopus laevis        ------------------------------------------------------------  0
Danio rerio           ---------------------------------------------MLLSKTHKHTGASSVS  16

Homo sapiens          FHPPAAMSERLRPRKR-RRNGNEEDNHLPPQTKRSS---RNPVFQDSWDTESS-------  109
Pan troglodytes       -------MEGSTIRKR-RRNGNEEDNHLPPQTKRSS---RNPVFQDSWDTETVPVMRNSK  49
Bos taurus            SSPSAAMSERLRPRKR-RRNGSEEDHHLPPQTKRSS---RNPVFHDSWDTESS-------  109
Rattus norvegicus     SPSPAAMSERLRPRKR-RRNGSDDDNHPPPQTKRSS---RNPIFQDSWDTESS-------  109
Xenopus laevis        ------ML--PDSRKR-RRNSNE-VSELPPSKRNT----WS-SELQEWETESS-------  38
Danio rerio           AGGSADMLTE--NRKRQRAEGDDEDAQMPQAKRLSSALQSSETARDSWESESS-------  67
                                *** * :..:   . *  .: :     .    :.*::*:

Homo sapiens          --------------GSDSGGSSSSSSSSINSPDRASGPEGS---LSQTMAGSSPNTPQPV  152
Pan troglodytes       ENRLRGNKAFCASSGSDSGGSS--SSSSINSPDRASGPEGS---LSQTMAGSSPNTPQPV  104
Bos taurus            --------------SSDSGGSSS---SSISSPDRASGPESS---LHHLAAGPGPHTPQPA  149
Rattus norvegicus     --------------SSDSGGSSS---SSINSPDRASGPESS---LSHIIPGSCPSTPQPM  149
Xenopus laevis        --------------GSES----S---NSNFSLERS--SCSE---TFQTMAGSGPATPQPV  72
Danio rerio           ----------------------SSESSWISSPDHAAGSTHCGGDVIGPPGGPGPCSPHSA  105
                                           .   * :::              *  * :*:

Homo sapiens          --PEQSALCQGLYFHINQTLREAHFHSLQHRGRPLT-  186
Pan troglodytes       --PEQSALCQGLYFHINQTLREAHFHSLQHRGRPLT-  138
Bos taurus            --PEPSALCQGPYFHINQTLKEAHFHSLQHRGRPPS-  183
Rattus norvegicus     --PEQSALCQGPYFHINQTLKEAHFHSLQHRGRPPT-  183
Xenopus laevis        SSPEQSALNRGPYVHINQILKEAHFSSLQQRCCNSS-  108
Danio rerio           SKPS-GPMDLLSYQHINRVLREAHFHSLQSRSQAKHR  141
                        *. . :    * ***: *:**** *** *
```

D

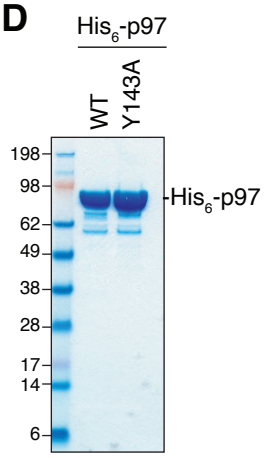

E

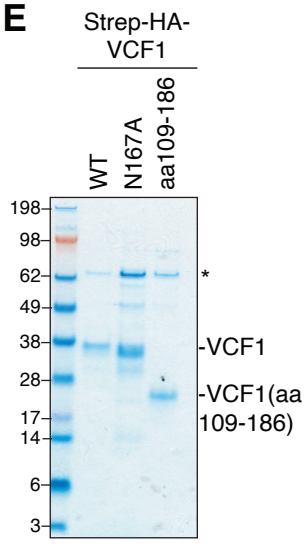

F

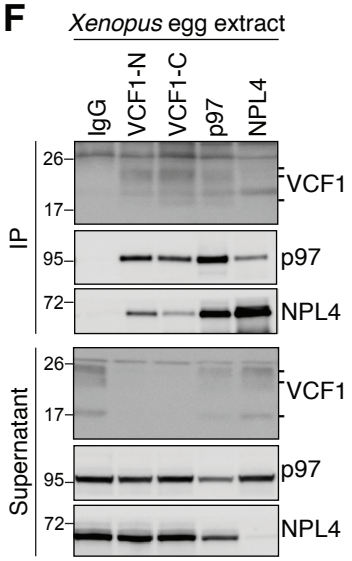

G

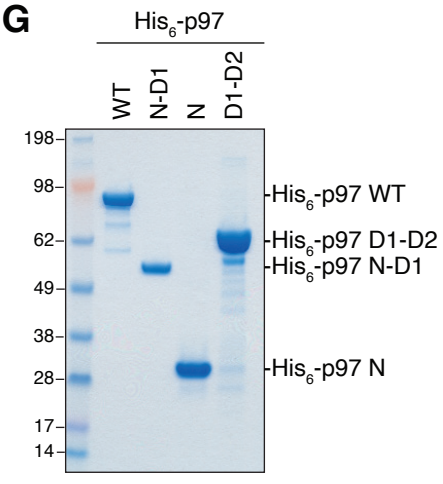

bioRxiv preprint doi: https://doi.org/10.1101/2023.07.25.550448; this version posted July 25, 2023. The copyright holder for this preprint (which was not certified by peer review) is the author/funder, who has granted bioRxiv a license to display the preprint in perpetuity. It is made available under aCC-BY-NC-ND 4.0 International license.

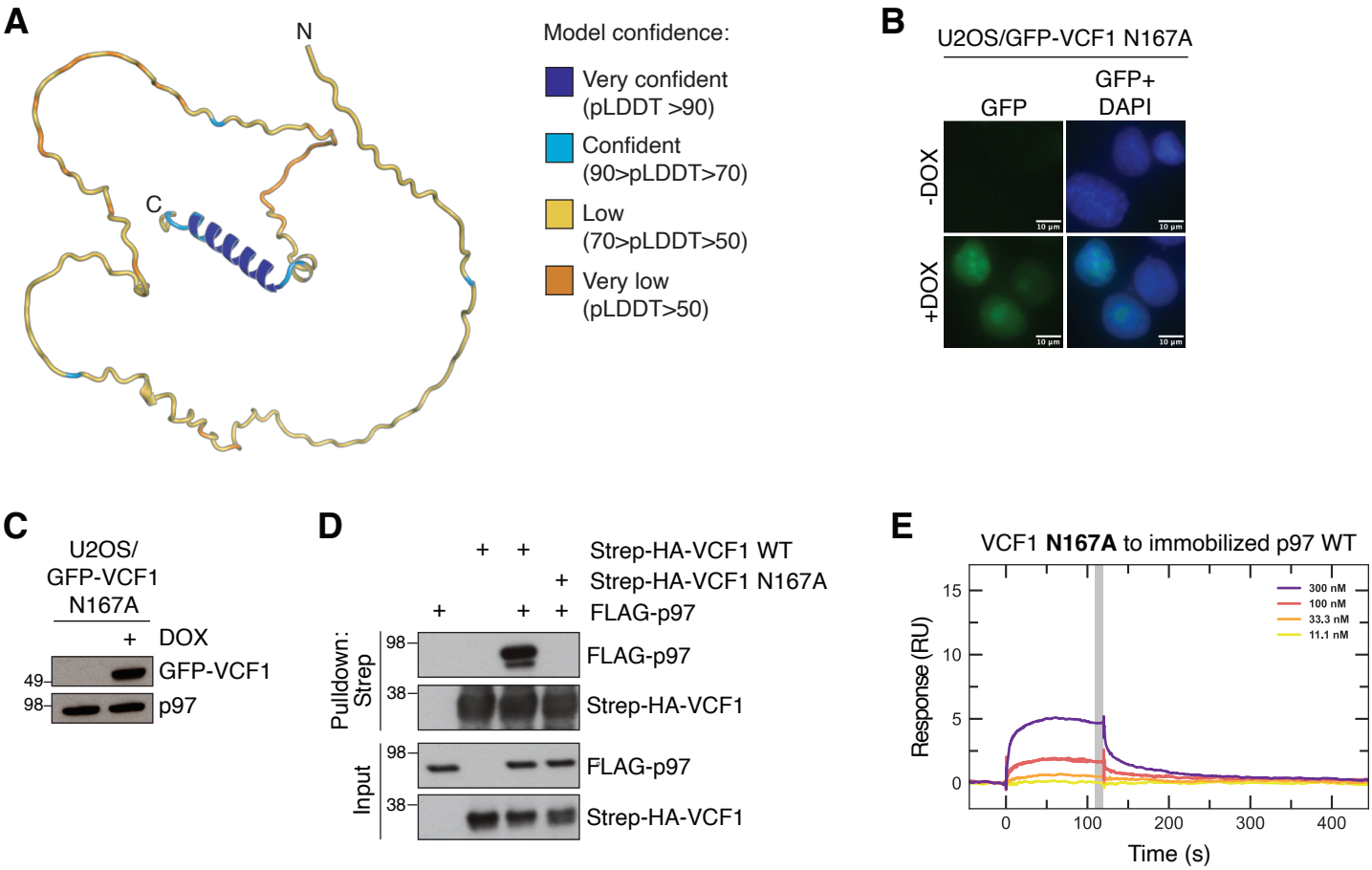

bioRxiv preprint doi: https://doi.org/10.1101/2023.07.25.550448; this version posted July 25, 2023. The copyright holder for this preprint (which was not certified by peer review) is the author/funder, who has granted bioRxiv a license to display the preprint in perpetuity. It is made available under aCC-BY-NC-ND 4.0 International license.

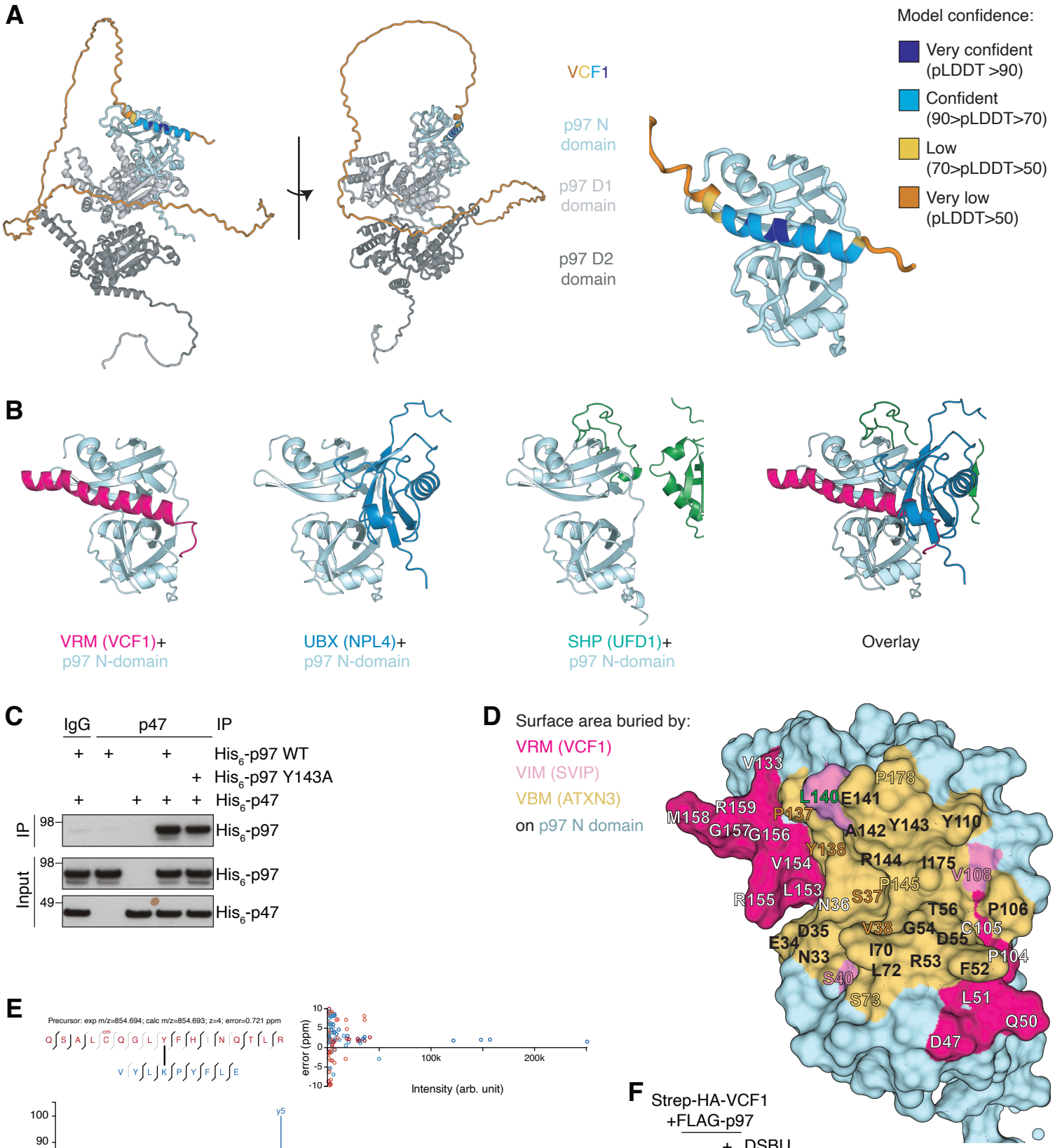

bioRxiv preprint doi: https://doi.org/10.1101/2023.07.25.550448; this version posted July 25, 2023. The copyright holder for this preprint (which was not certified by peer review) is the author/funder, who has granted bioRxiv a license to display the preprint in perpetuity. It is made available under aCC-BY-NC-ND 4.0 International license.

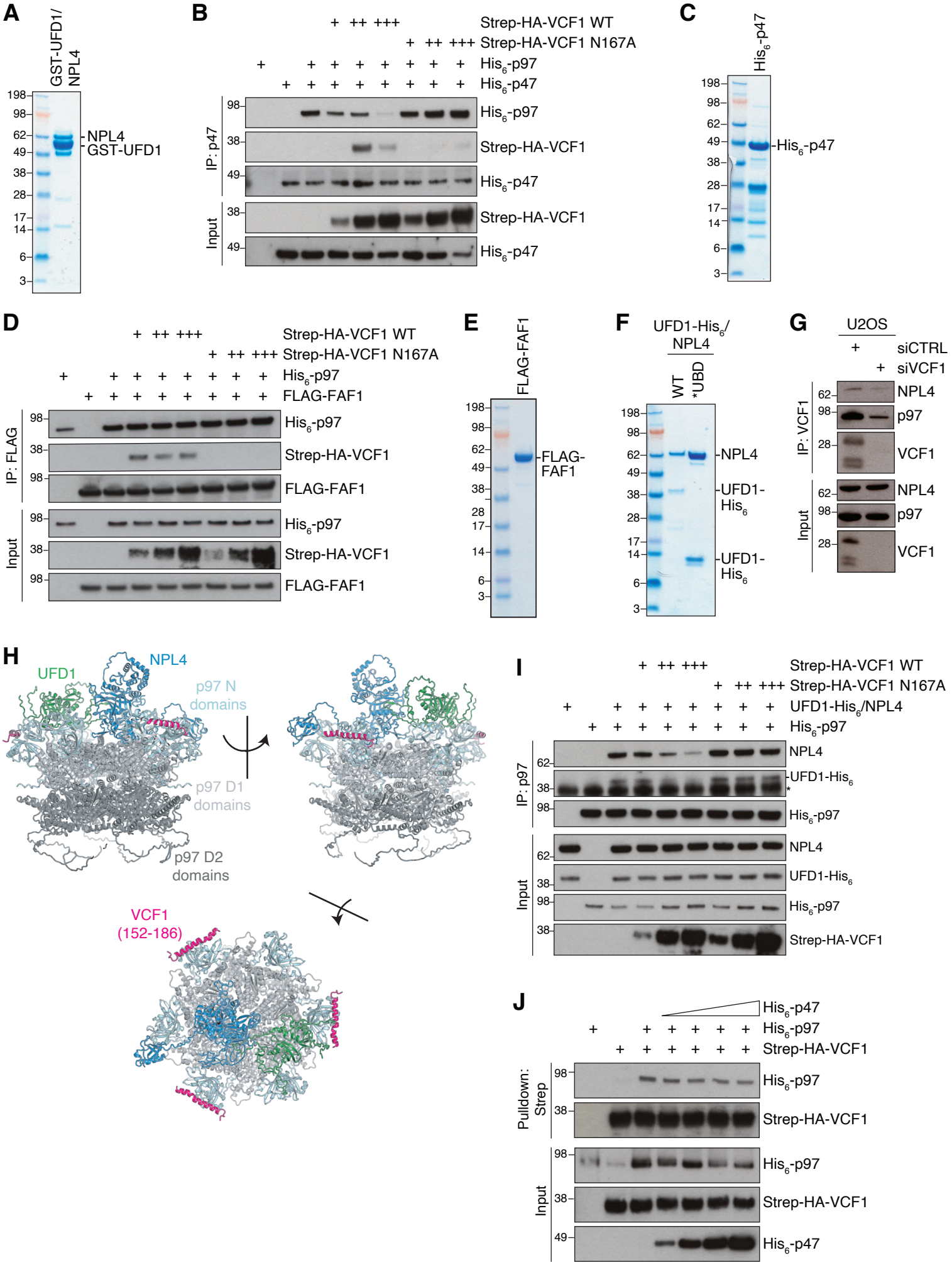

bioRxiv preprint doi: https://doi.org/10.1101/2023.07.25.550448; this version posted July 25, 2023. The copyright holder for this preprint (which was not certified by peer review) is the author/funder, who has granted bioRxiv a license to display the preprint in perpetuity. It is made available under aCC-BY-NC-ND 4.0 International license.